Energy Conversion and Management 321 (2024) 119023

Contents lists available at ScienceDirect

Energy Conversion and Management

journal homepage: www.elsevier.com/locate/enconman

Research Paper

Fluorobenzene as new working fluid for high-temperature heat pumps and organic Rankine cycles: Energy analysis and thermal stability test

M. Doninelli [a,*], G. Di Marcoberardino [a], I. Alessandri [b], C.M. Invernizzi [a], P. Iora [a]

[a] Università Degli Studi di Brescia, Dipartimento di Ingegneria Meccanica Ed Industriale, Via Branze, 38, 25123 Brescia, Italy
[b] Università Degli Studi di Brescia, Dipartimento di Ingegneria Dell'Informazione, Via Branze, 38, 25123 Brescia, Italy

ARTICLE INFO

Keywords:
Heat Pumps
ORC
Power Thermodynamic Cycles
Thermal stability
High Temperature
Working Fluids

ABSTRACT

Industrial high-temperature heat pumps and Organic Rankine Cycles play a pivotal role in reducing CO_2 emissions of the industrial sector. While several eco-friendly refrigerants have been explored for subcritical heat pumps below 150 °C, above this threshold only a few fluids can be adopted.

In this article, fluorobenzene (C_6H_5F) is proposed for the first time as a versatile working fluid suitable for both HTHP and ORC systems. Notably, it possesses a near-zero Global Warming Potential, null Ozone Depletion Potential, low cost, and low toxicity. The thermo-chemical stability of fluorobenzene is experimentally investigated with an advanced procedure, simulating the presence of the non-condensable-gases removal system in real plant operating conditions. The yearly rate of unimolecular decomposition is estimated less than 4 % at 350 °C, and even after 400 h of thermal stress no decomposition products have been detected in the liquid phase through Fourier Transform Infrared Spectroscopy.

In a direct heat exchange case study, coupled with exhaust gases at 390 °C, fluorobenzene achieves a net power production higher than other commercial fluids adopted in high-temperature units. In subcritical two-stage throttling heat pump condensing at 180 °C fluorobenzene shows a good Coefficient of Performance of 3.25 at 100 °C temperature lift.

1. Introduction

In recent years, industrial high-temperature heat pumps (HTHP) have gained significant attention for their role in decarbonising the industrial heat demand. According to Naegler et al. [1], in 2012, the final energy demand for heat across all EU28 member states accounts for 2077 PJ below 100 °C, 2214 PJ in the 100–400 °C range, and 3859 PJ above 400 °C. Steam generation constitutes approximately 40 % of industrial process heating demand in Europe [2], representing the predominant heat requirement from 100 °C up to 500 °C. The near future may see conventional steam boilers [3], fuelled by fossil sources, being replaced with high-temperature heat pumps, particularly in industries like pulp and paper and food and beverage, due to their substantial heat demand up to 200 °C [4].

Arpagaus et al. [5] provided for a comprehensive overview of high-temperature heat pumps, focusing on the temperature range below 150 °C due to current technological limitations. They identified the shortage of refrigerants combining high-temperature capabilities with low Global Warming Potential (GWP) as one of the major obstacle to the wider adoption of the HTHP technology in industrial sectors.

The selection of an appropriate working fluid is a crucial aspect in designing a heat pump system, resulting in a compromise among several factors. In fact, an ideal working fluid should possess thermodynamic and physical adequate characteristics, thermo-chemical stability (no or limited degradation at the operating temperatures), safety (non-flammable, nontoxic, nonexplosive), market availability, environmental characteristics (low GWP and near-zero ODP), and compatibility with materials and lubricants in the compressor (if not oil-free).

Historically, heat pumps have relied on hydrofluorocarbons (HFCs) and, more recently, hydrofluoroolefins (HFOs) as refrigerants. In compliance with EU climate objectives, the F-Gas regulation anticipates the industry's transition to alternative refrigerants characterized by a reduced Global Warming Potential (GWP). HFC-245fa, possessing a zero Ozone Depletion Potential (ODP) and a high critical temperature of 154 °C, was adopted in the past as a prevalent substitute for refrigerants like R114, R113, R123, and R500. Despite its widespread use, also in ORC systems, it's essential to acknowledge that HFC-245fa, with a Global Warming Potential ($GWP_{100\text{-years}}$) of 1030, is subject to phase-out requirements stipulated by pertinent regulations. Matheus-Royo et al. [6]

* Corresponding author.
E-mail address: m.doninelli002@unibs.it (M. Doninelli).

https://doi.org/10.1016/j.enconman.2024.119023
Received 18 June 2024; Received in revised form 2 September 2024; Accepted 3 September 2024
Available online 16 September 2024

Nomenclature

Acronyms

C	Compressor
COP	Coefficient of Performance, –
CSP	Concentrated Solar Power
EoS	Equation of State
EU	European Union
FTIR	Fourier-Transform Infrared Spettroscopy
GWP	Global Warming Potential
HP	High Pressure
HT	High Temperature
HTHP	High Temperature Heat Pump
HTF	Heat Transfer Fluid
LP	Low Pressure
MW	Molecular Weight
NBP	Normal Boiling Point
NCG	Non Condensable Gases
NFPA	National Fire Protection Association
ODP	Ozone Depletion Potential
ORC	Organic Rankine Cycle
PHE	Primary Heat Exchanger
PR	Peng Robinson
SP	Size Parameter, m
WHR	Waste Heat Recovery

Symbols

Δh	Enthalpy Difference, kJ/kg
ΔT	Temperature Difference, K
Δt	Time Difference, s
A	Area, m^2
Cp	Specific Heat Capacity at Constant Pressure
$\dot{m}$	Mass flow rate, kg s^{-1}
N	Number of experimental data points
P	Pressure, bar
PT	Pressure Transmitter
$\dot{Q}$	Thermal Power, MW
R	Gas Constant, kJ kg^{-1} K^{-1}
s	Specific Entropy, kJ kg^{-1} K^{-1}
T	Temperature, K
U	Global Heat Transfer Coefficient, W m^2 K
V	Volume, m^3
$\dot{W}$	Mechanical Power, MW
x	Mass Vapour Quality [-]
z	Compressibility factor, –

Greek symbols

η_{th}	Cycle Thermal Efficiency, –
$\eta_{is,C}$	Compressor isentropic efficiency, –
$\eta_{is,T}$	Turbine isentropic efficiency, –
$\eta_{is,P}$	Pump isentropic efficiency, –
ω	Pitzer acentric factor, –
ρ	Density, kg m^{-3}
σ	Molecular Complexity Parameter, –
π	Suface Tension, N m^{-1}
λ	Thermal Conductivity, W m^{-1} K^{-1}
η	Dynamic Viscosity, N s m^{-2}

Subscripts

cr	Critical
comp	Compressor
el	Electrical
i	property relative to the i-th experimental point
in	Inlet
int	Intermediate
is	Isentropic
L	Liquid
min	Minimum
max	Maximum
r	Ratio
red	Reduced
sat	Saturation
SH	Superheating
SV	Saturated Vapour
th	Thermal
v	property relative to the saturated vapour
vap	Vapour
vr	reduced property relative to the saturated vapour
wf	Working Fluid

assessed HCFO-1224yd(Z), HCFO-1233zd(E), and HFO-1336mzz(Z) as alternatives to HFC-245fa in high-temperature heat pumps, achieving a coefficient of performance (COP) of approximately 3 with a temperature lift (the difference between condensation and evaporation temperatures) of 70 °C. They also developed a prototype with a heat sink temperature of 140 °C using four low-GWP refrigerants [7]. a prototype that achieves heat sink temperature of 140 °C adopting four low-GWP refrigerants. Sulaiman et al. [8] explored various low-GWP refrigerants for subcritical heat pumps with condensing temperatures up to 140 °C. Carbon dioxide (CO_2) is one among the candidates for future high-temperature heat pumps [9], being operated in transcritical cycle with maximum (sensible) sink temperature around 130 °C. Compressed carbon dioxide energy storage system (CCES) [1011] can be integrated with CO_2 heat pumps to improve the round trip efficiency [11]. Liu et al. [12] also explored the use of CO_2 mixtures with R134a, R290, R600 and R601 to improve the efficiency of a pumped thermal energy storage by exploiting the temperature glide during the phase transition of the zeotropic mixtures.

HFO-1336mzz(Z) is being considered as an alternative to R-245fa in high-temperature, high-pressure (HTHP) applications. Notably, it's the only high critical temperature fluid (above 170 °C) with low global warming and zero ozone depletion potential, making it a practical and sustainable choice for HTHP. The thermal stability limit of HFO-1336mzz(Z) has been investigated by Kontomaris et al. [13], assessing that the fluid is chemically stable up to 250 °C, as HFC-245fa, suggesting its application in medium–low temperature ORC systems. Navarro-Esbrí and Mota-Babiloni [14] experimentally demonstrated that the fluid is capable to produce useful heat above 155 °C, when coupled with a sensible heat source at 100 °C.

In his review work, Arpagaus [5] indicated R1336mzz(Z), R718, R245fa, R1234ze(Z), R600, and R601 as suitable fluids to achieve high heat sink temperatures of up to 160 °C. Also, Dai et al. [15] carried out techno-economic analysis considering R1234ze(Z) limiting to sink temperatures up to 120 °C. However, above the 150–160 °C delivery temperature, it is difficult to find suitable working fluids due to critical temperature, thermal stability, and compressor issues. Despite this, there is large industrial demand even above 160 °C that should be covered by the HTHP technology. As an example, the chemicals sector in the U.S has around 62 % of the heat demand in the temperature range from 160 to 200 °C [16], which is beyond the operative temperature limits of the mentioned refrigerants. HFOs could be applied in this temperature range in transcritical conditions which do not match well with most of the industrial heat demand being covered by high-quality steam production (isothermal). Moreover, there are some concerns

about the thermal stability of some HFOs above 170 °C. For instance, HFO-1234yf thermally degrades at 170 °C [17], while the pyrolysis temperature of R1234ze(E) starts occurring around 230 °C [18].

Few studies have been conducted about subcritical HTHPs delivering heat above 150 °C, most of which deals with transcritical refrigerants [1920] or subcritical zeotropic mixtures [212223], that match well only with sensible sinks. A good overview of the industrial efforts about steam generating heat pumps condensing above such temperature threshold is presented in the work of Klute et al. [24]. The most considered solution to delivered high-temperature steam is to manufacture a cascaded cycle where the bottoming cycle is a closed-loop compression heat pump, and the top cycle is mechanical vapour recompression (MVR) producing high-pressure steam. As an example, a commercial solution [25] considers R1336mzzz(Z), R1224yd(Z), or R1233zd(E) as refrigerant for the bottoming cycle, equipped with centrifugal compressors.

The research of appropriate working fluids is even complicated by the restrictions that many fluids will face in the near future at least in Europe. According to the proposal of October 2022 of the European Council [26], from 1st January 2033 Split systems of a rated capacity of more than 12 kW based on fluorinated greenhouse gases with GWP of 150 or higher will be banned. Newly developed hydrofluoroolefins (HFOs) and hydrochlorofluoroolefins (HCFOs), given the low GWP, emerge as viable options for heat sinks below 160 °C. However, it's important to note that anticipated EU restrictions on fluorinated olefins in the near future emphasize the pivotal significance of carefully choosing the working fluid.

In fact, in January 2023, the national authorities of the Netherlands, Germany, Sweden, Denmark and Norway submitted their Restriction Proposal to the European Chemicals Agency (ECHA). The proposal aims to restrict manufacturing, the placing on the market (including import) and the use of polyfluoroalkyl substances (PFAS) in Europe. The list covers over 10,000 substances, including Fluorinated gases (F-gases) and fluoropolymers that are used for heat pump equipment. As an example, 3 M company will exit all PFAS manufacturing by the end of 2025. Structures subjectively considered to be PFAS were composed of either 30 % or 40 % fluorine, based on the fraction of the molecular formula excluding hydrogen atoms [27].

In this context, there is need to look for alternative working fluids that do not face F-Gas or PFAS restrictions. Especially in the temperature range above 160 °C, a research gap about suitable refrigerants exists. Abedini et al. [28] underlined how suitable refrigerants for high temperature (up to 200 °C) are not yet available, and for this reason they proposed binary mixtures as working fluid. However, mixtures deliver sensible heat, which is a niche market in the industry where heat is mostly required at constant temperature. The 160 °C barrier is overcome by Turboden company, showcasing the possibility to deliver heat up to around 200 °C, by adopting HCs as working fluids: cyclopentane, n-pentane, and isopentane are adopted in the 160–200 °C temperature range due to high critical temperature. The necessity to shift from simple molecules (such as conventional refrigerants) to complex fluids (as highly-branched HCs), commonly used in ORC systems, in the context of HTHP approaching 200 °C, was well anticipated by Angelino and Invernizzi [29] in 1987.

In this context, pure fluorobenzene (C_6H_5F) is proposed for the first time in this article as potential working fluid to be applied both in closed-loop HTHPs and ORC systems. With one single fluorine atom in the molecule, fluorobenzene is not classifiable as PFAS substance, according to the abovementioned classification. Moreover, it possesses near-zero GWP ($GWP_{100\text{-}years} \ll 1$), as reported by Burkholder et al. [30], and zero ODP, making it an environmental-friendly working fluid. Additionally, the exceptionally-high critical temperature (286 °C) suits well the HTHP application, making it suitable to cover even the temperature range above 160 °C where new-generation low-GWP refrigerants cannot cover in subcritical configuration. Unlike its hydrocarbon counterpart benzene, fluorobenzene has much lower toxicity. When compared to hexafluorobenzene (C_6F_6), instead, fluorobenzene is much cheaper (about 1/10th the cost of C_6F_6 for a quotation of around 1 kg quantity). The main thermophysical properties of fluorobenzene are presented in Table 1, such as molecular weight (MW), normal boiling point (NBP), but also density (ρ), dynamic viscosity (η), thermal conductivity (λ), latent heat of vaporization (Δh_{eva}), surface tension (π), liquid heat capacity (Cp_L) experimentally available in literature at near ambient conditions (20 °C).

To confirm its potential application as working fluid, it is of fundamental importance to assess the thermo-chemical stability. In this paper, the consolidated static survey method adopted in the past for several ORC working fluids [37] and refrigerants [38] have been adopted. This method is particularly relevant since decomposition phenomena are detected from divergence of vapour pressure of the thermally stressed fluids in comparison with the fresh fluid, so it provides also useful indications about the fluid behaviour during system operation. The increase of vapour pressure due to the formation of decomposition products, constituted in prevalence of non-condensable-gases (NCG), reduces the available enthalpy drop across the turbine of an ORC reducing the overall performance [39]. A NCG removal system is commonly employed in ORC systems when dealing with subatmospheric condensation pressure at design conditions [40], i.e. with fluids characterized by high normal boiling point as it is fluorobenzene (86 °C). The working fluid in the hot-well, affected by the presence of NCGs, is extracted though a vacuum pump and in the NCG removal system a gas treatment unit facilitates the recovery of a portion of the working fluid, which is then reintroduced into the power block [41].

In this article, compared to previous literature works, the thermal stability of the working fluid has been evaluated also simulating the presence of the NCG removal system in real ORC operations. The thermally stressed fluid is aspirated for a short time to remove the vapour phase in the test cylinder, and the vapour pressure of the fluid is evaluated and compared to the fresh fluid behaviour. This test is finalized to prove that decomposition products are only in the vapour-phase and the fluid recirculated from the NCGs removal system into the power block maintains its physical and chemical properties unchanged. Additionally, this is also confirmed by a chemical analysis with Fourier-transform infrared spectroscopy (FTIR) on the liquid phase, after undergoing prolonged thermal test.

As the experimental campaign evidences a good thermo-chemical stability of fluorobenzene, degrading below 4 % annually at 350 °C, a case study considering its use in an ORC system directly coupled with industrial exhaust gases at 390 °C is investigated. The exergy efficiency attainable with the adoption of fluorobenzene in this context is evaluated and compared with the few other organic fluids thermally stable at this temperature level. The specific application of direct heat exchange has been selected, compared to the more conventional indirect heat transfer through thermal oil loop, as fluid overheating (hot spot) and consequent decomposition are more likely to occur, especially during the transient operation of ORC at conditions of high heat flux [42].

The key novelty contributions of the present article can be summarized in:

- Pure fluorobenzene is presented for the first time as working fluid for HTHP and ORC systems.
- The thermal stability of fluorobenzene is experimentally investigated with a consolidated procedure.
- An advanced methodology has been developed to assess the thermal stability of the fluid simulating the presence of a NCG removal system in real ORC operation.
- A chemical analysis with FTIR methodology is performed on the thermally stressed fluorobenzene confirming no traces of degradation products in liquid phase.
- The annual degradation rate at 350 °C of fluorobenzene is measured and compared to other high-temperature working fluids.

Table 1
Main thermophysical properties of fluorobenzene.

Property	MW	ρ (20 °C)	NBP	λ (20 °C)	η	Δh_{eva} (20 °C)	π (20 °C)	Cp_L (20 °C)
Units	kg mol^{-1}	kg m^3	°C	W m^{-1} K^{-1}	μPa s	MJ kmol^{-1}	N m^{-1}	MJ kmol^{-1} K^{-1}
Value	0.961	1022.5 [31]	84.7 [32]	0.137 [33]	585 [NIST Database]	345.2 [34]	0.0227 [35]	0.146 [36]

- The performance of fluorobenzene in subcritical HTHP delivering heat at 180 °C (a thermal level poorly explored in the literature) is studied in different cycle architectures, providing useful insights about different working fluids.
- The efficiency gain deriving from the application of fluorobenzene in ORC in direct heat exchange with flue gases at 390 °C, in comparison to other fluids commercially adopted in high-temperature ORC units.

2. Experimental investigation

2.1. Thermal stability test: Setup and procedure

In this work, the consolidated static isochoric method developed by Invernizzi et al. [43] to evaluate the thermo-chemical stability of working fluids for Organic Rankine Cycles (ORC) has been adopted with the addition of a novel approach consisting of simulating the effects of NCG removal system as present in many commercial ORC systems.

The static survey method has been adopted in the Fluid Test Laboratory [44] with several working fluids in the past such as hydrocarbons [3745], zero-ODP refrigerants [38], fluorinated alchols [46], perfluorocarbons [47], and CO_2 mixtures with perfluorocarbons [48]. It is based on the concept that even a small breakdown of the fluid can cause an appreciable rise in vapor pressure due to presence of decomposition products. In fact, due to prolonged exposure to thermal stress at a temperature surpassing the activation energy barrier, the molecules undergo fragmentation into smaller, more volatile compounds. The identification of degradation phenomena is achieved through a comparative analysis of vapor pressure variations post thermal stress against the baseline of the fresh fluid (reference vapour pressure curve).

The experimental setup and procedure is well presented in the work of Pasetti et al. [37]. The specific setup used in this work is presented in Fig. 1. The main component of the system is the sample cylinder ("A" in Fig. 1), manufactured in AISI 316L, a material commonly employed in power plant components, whose internal volume is 150 cm^3. The tubes and valves illustrated are made of the same material. Consistent material choice for all components in the high-temperature sections is crucial, as it can potentially catalyse the decomposition reaction of the fluid.

Two pressure transducers are mounted in the systems to have high accuracy in the entire pressure measurement range. It is particularly important to have accuracy as much as possible in the pressure range where the reference vapour pressure is measured, and for this reason it is measured through a Klay 2000-SAN pressure transmitter ("PT1" in Fig. 1) with adjustable span from 1 to 10 bar and accuracy of 0.1 % of adjusted span. When the cylinder is placed in the muffle furnace for the 100-hour thermal stress, the valve "V2" in Fig. 1 is closed to protect the low-pressure transmitter from overpressure. In that case, the pressure is recorded by using the high-pressure transmitter ("PT2" in Fig. 1), a Klay 2000-SAN with adjustable span from 20 to 100 bar. A Tersid thermocouple (tolerance class I) is inserted into the cylinder through its welded housing ("B" in Fig. 1). The main instruments, with related accuracy, are listed in Table 2.

The cylinder is loaded with 30 g of liquid fluorobenzene: the fluid is supplied by Merck [49] with a declared purity level above 99 %.

The static isochoric thermal stability test involves the following steps: (i) utilizing a vacuum pump to eliminate air and impurities; (ii) introducing a fresh fluid sample of arbitrary mass (but sufficient to have vapour-liquid equilibrium conditions) into the closed cylinder; (iii) placing the cylinder in a thermostatic bath to measure vapor pressure at various temperatures (establishing a reference curve); (iv) placing the cylinder horizontally in a muffle furnace to carry out a 100-hour constant-temperature stress test; (v) post thermal stress, re-evaluating vapor pressure within the same temperature range, as the reference curve, in the thermostatic bath; (vi) subjecting the fluid to a new thermal stress at a higher constant temperature; (vii) iterating the procedure until reaching the maximum test temperature.

There are various reasons to conclude the test at a certain temperature: i) after thermal stress at that temperature, the fluid decomposition

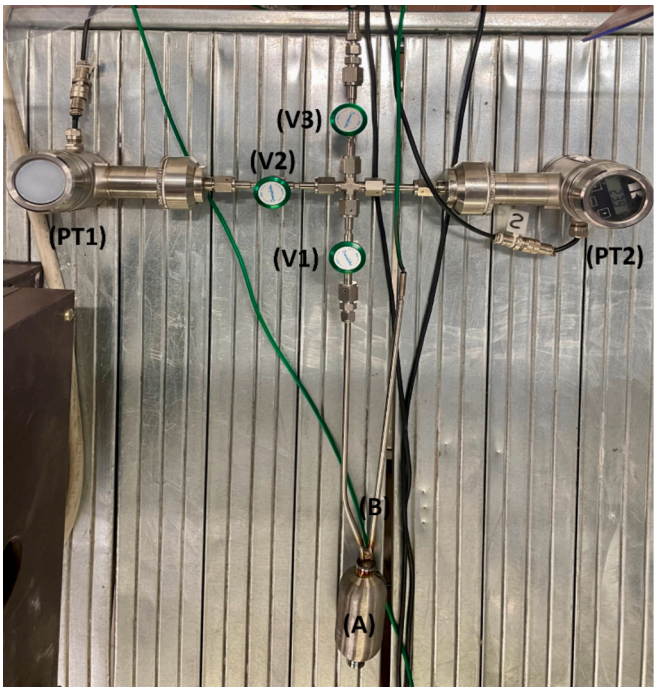

Fig. 1. Main components of the thermal stability test. the AISI 316L cylinder (A), the housing of the temperature probe (B), the low-pressure scale pressure transducer (PT1), the high-pressure scale pressure transducer (PT2), the main valve that closes the cylinder from the rest of the circuit (V1), the valve which protects the PT1 from overpressure (V2), the valve that connects the circuit to the environment (vacuum pump/charging/venting).

Table 2
Instruments for thermal stability testing and related accuracy.

Type	Manufacturer	Model	Measurement range	Accuracy
Pressure transmitter 1	Keller	Klay 2000-SAN	0..10 bar*	0.1 % of full-scale
Pressure transmitter 2	Keller	Klay 2000-SAN	0..100 bar*	0.1 % of full-scale
Thermocouple	Tersid	Type K	−200–1270 °C	Tolerance class I

* Adjustable span (1–10 bar for transmitter 1, 20–100 bar for transmitter 2).

appears significant (with high vapor pressure deviations); ii) there is practical interest in testing up to that temperature from an application perspective.

In this work, the decision to conclude the stability test was made upon reaching a thermal stress temperature of 350 °C for the following reasons: i) it represents a thermal threshold at which the vast majority of organic fluids decompose at a high rate and are, for this reason, impractical for use, with a few exceptions such as cyclopentane and toluene [37]; ii) it is a thermal level compatible with multiple applications (high-temperature waste heat, concentrated solar power CSP, biomass); iii) the objective is not to subject the fluid to complete degradation but rather to assess its real applicability at 350 °C by conducting further test as detailed in the following section.

2.2. Broadening the scope of the experimental investigation

In comparison to prior thermal stability investigations conducted in the Fluid Test Laboratory, the conventional methodology is here embedded within a broader framework, represented in Fig. 2.

The 1st stage of the experimental campaign consists of the conventional thermal stability test, detailed in previous section, up to the defined limit of 350 °C. In the 2nd stage, the fluid decomposition at the set temperature limit (350 °C) is monitored over time with consecutive 100-hours thermal stress up to 300 h. Concurrently, both at the beginning and at the end of this 2nd stage, verification is carried out to ensure that, following a brief aspiration (a few seconds with vacuum pump) of the fluid into the cylinder after the 350 °C thermal stress, its volumetric behaviour reverts to that of the fresh fluid. This procedure aims to identify any significant breakdown products in the liquid phase, ensuring confidence that any decomposition products formed in the high-temperature sections of the power block, subsequent to the removal of non-condensable gases, are completely eliminated. Consequently, upon reintroducing the recycled fluid from the NCG removal system, it retains its original thermophysical characteristics. This implies that the fluid at the pump does not appear affected by operating at 350 °C as the turbine inlet temperature.

After this second stage, as in Fig. 2, A chemical analysis on the thermally-stressed liquid after the "stage 2" was carried out to confirm the absence of decomposition products in the liquid phase. A Fourier-transform infrared spectroscopy (FTIR), using an Attenuated Reflection Setup (ATR, Everest Diamond-Thermo Nicolet) with a spectral resolution of 4 cm^{-1}, is used: the FTIR measurements were carried out by dropping 5 μL of liquid on a diamond ATR crystal. After the subtraction of the environmental background, the final spectrum was extracted as the average of 64 scans.

Despite qualitative indications about the thermal degradation of the fluid occurring in the 1st and 2nd stages are evident from Figs. 3 and 4, a semi-quantitative index, the so-called quasi-constant rate of decomposition k* of the fluid, following the same methodology as explained in the work of Invernizzi et al. [45]. In the mentioned work, the authors measured the decomposition rate of n-pentane, cyclopentane and toluene after eighty hours thermal stress at varying temperatures. The same conceptual methodology is used in this work to calculate the decomposition rate k* of fluorobenzene, and to compare it with other fluids.

As stated in [45], the unimolecular decomposition typically manifests as an increase (ΔP_v) in the vapor pressure of the sample fluid, especially appreciable under sub-atmospheric conditions. This article introduces two methodological differences, compared to [45], for determining the decomposition rate k*: (i) the rate k* following thermal stress at a specific temperature is calculated based on the ΔP_v at that temperature in relation to the preceding thermal stress (usually performed at a lower temperature), rather than comparing it to the vapor pressure of the reference fresh fluid. The adjustment is incorporated in this study to attribute the formation of decomposition products exclusively to the latest thermal stress (latest temperature), excluding the influence of previous thermal stresses carried out at different temperatures/conditions. This new approach is graphically addressed in Appendix, where the main equations for the calculation of k* are also presented.

As outcomes of the 1st stage of thermal stability testing, it is possible to evaluate the rate of decomposition of Fluorobenzene k* as function of temperature up to 350 °C.

Slater's theory [29] suggests that a gas of polyatomic molecules acts as vibrating systems, dissociating when one internal coordinate exceeds a critical value tied to dissociation energy. The energy required for this dissociation, mainly driven by temperature, depends on the molecules' kinetic energy and collision force. Hence, the degradation rate (k*) of the working fluid is primarily influenced by the maximum temperature, however in this article the effect of the time on the kinetic of reaction has been investigated. In fact, the 2nd stage provides insights into the temporal evolution of the degradation rate k* specifically at 350 °C.

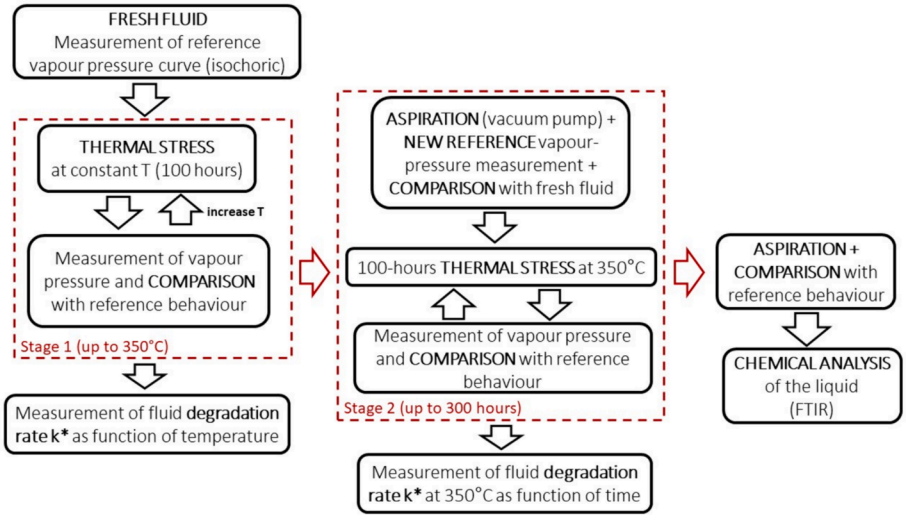

Fig. 2. Methodology adopted for the experimental investigation on fluorobenzene, comprising. i) at first stage, the consolidated static survey method for thermal stability testing up to 350 °C; ii) at second stage, the evaluation of degradation phenomena at 350 °C at 100-hours' time step up to 300 h, with vapour aspiration to evaluate the presence of decomposition products in liquid phase; iii) the final evaluation of the thermally stressed liquid fluorobenzene with FTIR analysis after aspiration and check with reference curve.

2.3. Experimental results

The investigation focuses on measuring the reference vapor pressure below the normal boiling point of fluorobenzene (84.7 °C) where the effect of non-condensable products are more noticeable at vapor pressures below atmospheric pressure. Specifically, the temperature range from 10 °C to 80 °C has been considered, with steps of 10 °C (Fig. 3).

The measured vapor pressure curve of the fresh fluorobenzene, assumed as reference in the experimental analysis, and the fluid behaviour after thermal stress test are shown in Fig. 3. In the 1st stage, the sample fluid experienced four consecutive stress tests at temperature from 250 °C to 350 °C. At the end of each 100-hours stress test, the saturation pressure curve was measured, and compared with that of the virgin fluid in order to detect possible signs of decompositions.

For clarity purposes, uncertainties are not depicted on the graph because they would overlap with the data points, hindering a proper understanding of deviations of vapor pressure after different thermal stresses. There are two contributions of uncertainty related to each point in Figs. 3-4: the instrumental uncertainty and the standard deviations. As the pressure transmitter is set at 1 bar full scale, its resulting accuracy is 1 mbar. Each set of (P, T) values is calculated as the arithmetic mean of the data recorded over a 15-minute period at steady-state conditions, encompassing approximately 180 acquisition samples. The resulting standard deviation σ_P is within the instrumental uncertainty as the maximum standard deviation computed in 0.9 mbar. As the pressure transmitter is set at 1 bar full scale, its resulting accuracy is 1 mbar. The total uncertainty on the pressure values in Fig. 3 and Fig. 4 is typically below 2 mbar, then almost negligible, reaching 4 mbar as maximum value. In Appendix A it is possible to find the uncertainty of each measured point.

Fluorobenzene exhibits good thermal stability in the investigated temperature range (250–350 °C), as the deviations against the reference vapour pressure curve does not increase exponentially with temperature, unlike many other organic fluids [3746]. The increase in vapor pressure from one thermal stress to the next is linear, reaching a maximum value of 0.045 bar after thermal stress at 350 °C. A semi-quantitative comparison with other fluids for ORCs will be presented in this section based on the quasi-constant rate of decomposition reaction k*. The methodology adopted to calculate the k* parameter is detailed in the Appendix B. An example with toluene, in Appendix B, provides a clear indication of how the results of a thermal stability test translate into the estimate of the fluid degradation rate trend k*. Specifically, the example demonstrates that from the thermal stability results, it is evident when the fluid is undergoing significant degradation when vapour pressure deviations between successive stresses increases exponentially.

During the second stage of the experimental campaign, following the last 100-hours thermal stress conducted at 350 °C during the first stage, a brief aspiration of the fluid using the vacuum pump (few seconds) is performed to simulate the NCG removal system typically present in an ORC system. Subsequently, the vapor pressure of the fluid is measured to establish a new reference curve ("NEW REF" in Fig. 4): the resulting trend, equal to the reference of the fresh sample, suggests that all thermal decomposition products are light and incondensable substances at the investigated temperature. On the other way around, substances dissolved in the liquid phase of the fluorobenzene would contribute to a change in the vapour pressure compared to the pure fresh fluid sample. The second stage aims at investigating the progression of degradation over time (up to 300 h) with three additional 100-hours thermal stresses at the threshold value of 350 °C.

The 2nd stage of the thermal stability test confirms the low degradation rate of fluorobenzene at 350 °C, reasonably supporting its suitability for use in closed power cycles operating at this thermal level. Indeed, after 300 cumulative hours of thermal stress at 350 °C, the deviations from the reference curve are lower compared to the deviations measured at the end of the first stage at the same temperature, confirming the low rate of thermal decomposition reaction. Finally, the effect of the NCG removal system was simulated again by briefly aspirating with the vacuum pump and remeasuring the vapor pressure. The outcome of this procedure indicates that the fluid has returned to the

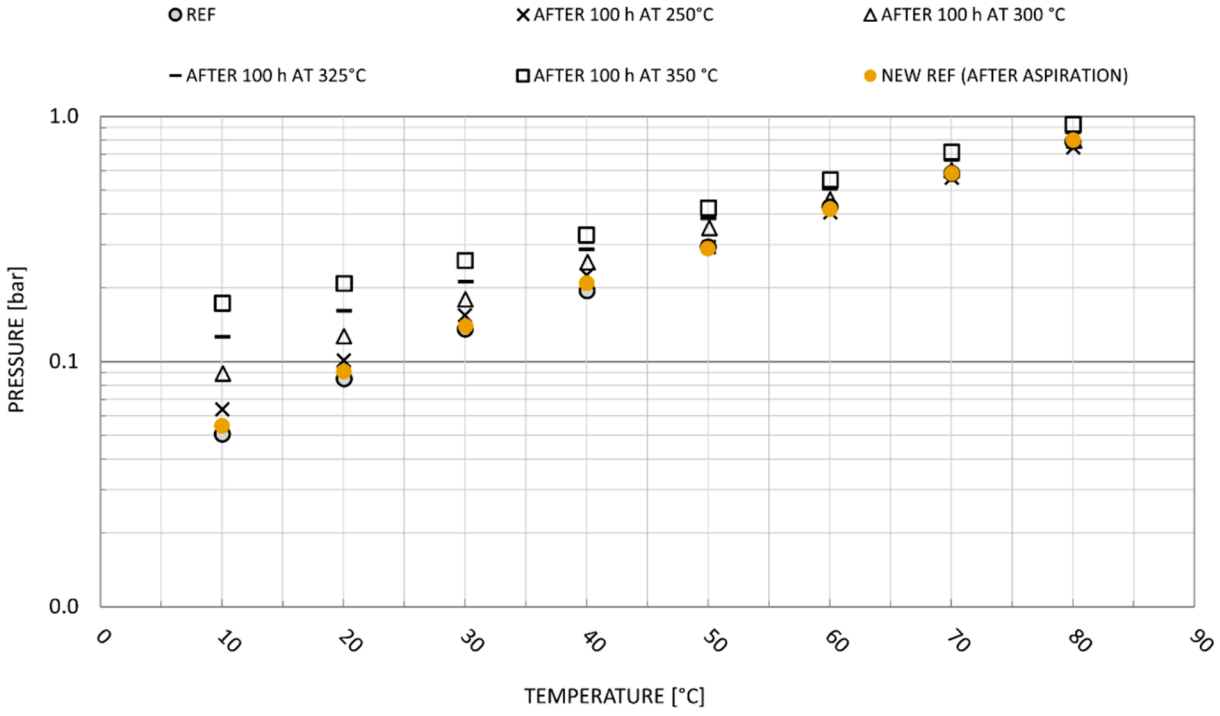

Fig. 3. Results of the 1st stage of thermal stability test on fluorobenzene, with the measured reference vapour pressure ("REF") and the vapour pressures measured subsequent 100-hours thermal stress at different temperatures (log scale); after the last 100 h at 350 °C, vacuum pump aspiration was performed and a new reference line ("NEW REF"), consistent with the previous one, was measured.

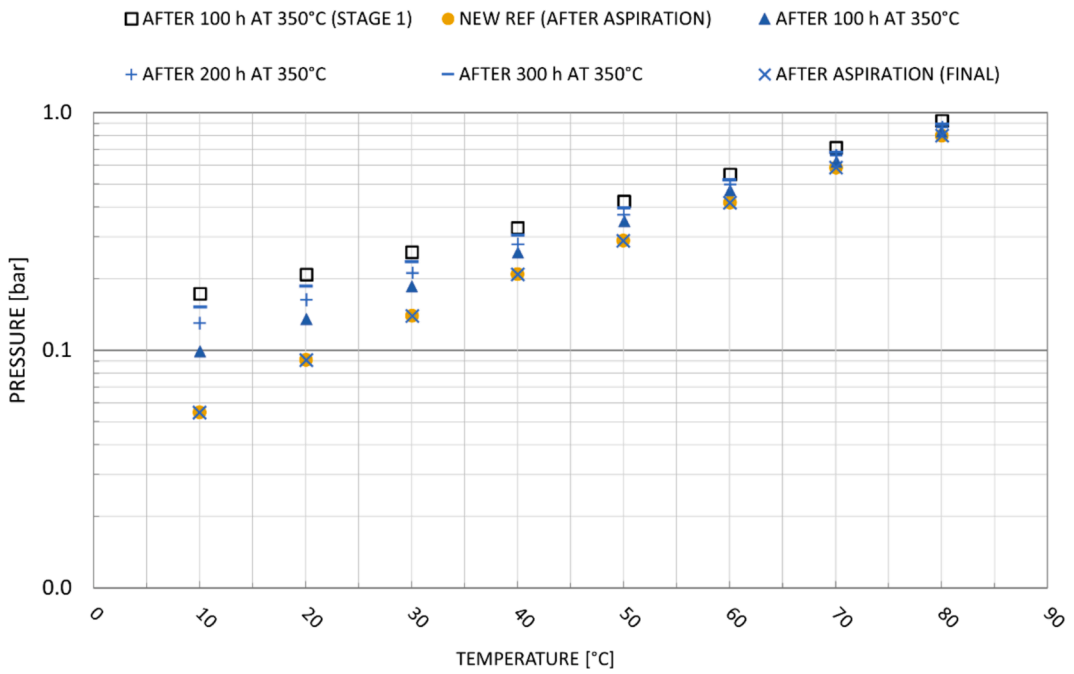

Fig. 4. Result of the 2nd stage of thermal stability test on fluorobenzene performed at 350 °C for several hours (following stage 1 previously described); before starting the 2nd stage, aspiration with vacuum pump is performed and a new reference line is established ("NEW REF"). After 300 h at 350 °C the pressure of the system results to be lower than the values measured before aspiration after 100-hours stress at the same temperature (squares); in the end of the test, the final aspiration with vacuum pump determined the fluid sample to return to the reference behaviour of the fresh fluid.

volumetric behaviour of the fresh fluorobenzene, further confirming that thermal stress does not influence the liquid reintroduced into circulation after NCG removal system.

Eventually, to definitely prove this result, a FTIR analysis of the liquid phase at the end of the entire thermal stability test was conducted by ATR. As shown in Fig. 5, the comparison between the FTIR spectra of fluorobenzene before (in blue) and after thermal stress (in red) does not reveal any significant difference: the two spectra are separated for clarity purposes shifting the red spectrum upwards (+0.4 absorbance units).

Eventually, Fig. 6 show the rate of decomposition reaction k* as function of temperature and time (at 350 °C), as outcomes of the 1st and 2nd stages of thermal stability testing. The semi-quantitative analysis provides indications on the velocity and the extent of the fluid degradation, but it is more useful to compare and classify the behaviour of different thermal-stressed working fluids.

At the end of the last thermal stress (350 °C) of 1st stage of the campaign, the quasi-constant rate of decomposition is 0.13×10^{-8} [s^{-1}] as evident from Fig. 6, meaning 4 % annual degradation of fluorobenzene at this temperature. Following aspiration and re-start with the 2nd stage (right side of Fig. 6), the k* approaches 0.14×10^{-8} [s^{-1}] after the first 100-hours at 350 °C, that is a value coherent with that obtained at the same temperature during the 1st stage. The value is slightly higher, after 100 h of the 2nd stage, because aspiration is performed at the end of the 1st stage: all the degradation products are removed from the system, and the reaction is then promoted as a consequence. For the same reason, in Fig. 6 (on the right) the rate of decomposition appears to decrease with time at constant temperature (350 °C): the accumulation of degradation products inhibits the unimolecular reaction (Le Châtelier's principle). For this reason, after prolonged thermal stress (300 h) of fluorobenzene at 350 °C, the decomposition rate stabilises at an asymptotic value of 0.0728×10^{-8} s^{-1}.

It's noteworthy that the calculation of the k* parameter assumes that 1 mol of decomposition products is generated from 1 mol of fluid, as discussed in Pasetti et al. [37]. This assumption is conservative, as the breaking of molecular bonds more readily leads to the generation of multiple moles of products from a single mole of fluid. This implies that the reported results on the k* rate are likely overestimated and should be scaled according to the actual reaction stoichiometry. The comparison of fluorobenzene with other working fluids, investigated in the same laboratory under the same assumptions, is presented in Fig. 7: these rates were determined using the same methodology outlined in the previous section and in Appendix B.

According to Fig. 7, fluorobenzene (as well as toluene and cyclopentane) degrades by less than 5 % per year at 350 °C. Moreover, no exponential trend of k* (discussed in Appendix B) is noticeable from the results of fluorobenzene in the investigated temperature range. Further test, at higher temperature, could identify the temperature above which

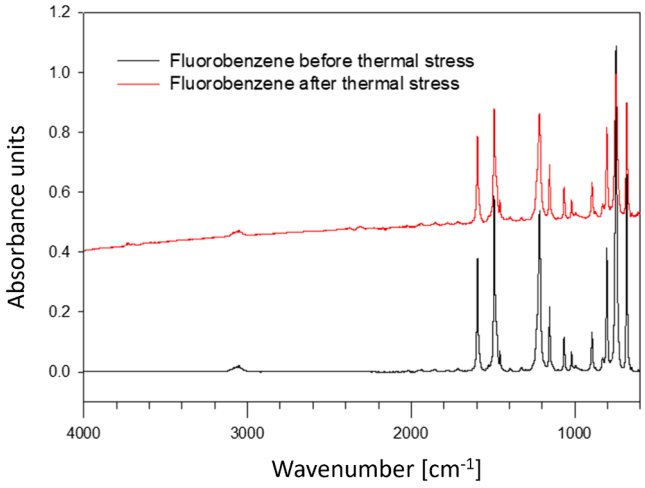

Fig. 5. ATR-FTIR spectra of fluorobenzene before (blue, reference from Aldrich Library. Fluorobenzene > 99 %) and after (red) thermal stress; the two spectra are shifted upwards for clarity purposes. (For interpretation of the references to colour in this figure legend, the reader is referred to the web version of this article.)

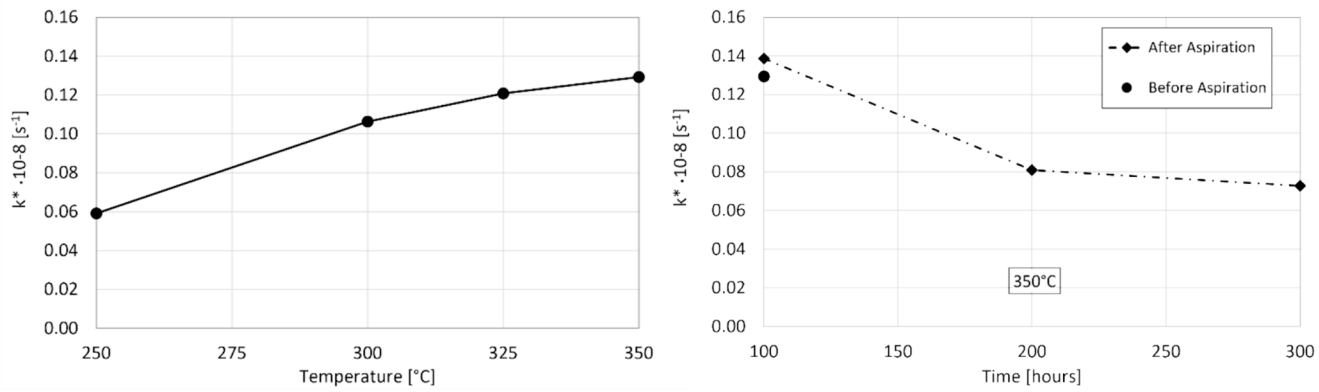

Fig. 6. Fluorobenzene degradation rate k* as function of temperature (left) from the 1st stage, and time (right) from the 2nd stage at 350 °C thermal stress.

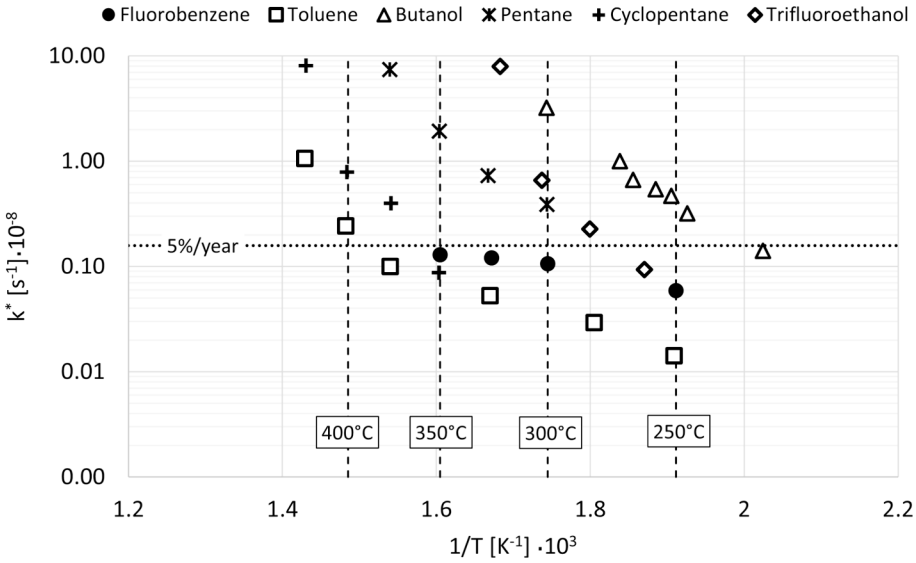

Fig. 7. Rate of unimolecular decomposition reaction of fluorobenzene at different temperatures in comparison with other fluids precedingly tested in our Fluid Test Laboratory with the same isochoric method [37].

exponential trend of k* is noticeable. This result is encouraging for the application of fluorobenzene in high-temperature ORC units, where the working fluid could be coupled with medium–high temperature sources in direct heat exchange.

3. Fluorobenzene as working fluid in ORC in direct heat exchange

Given the good thermal stability of fluorobenzene, demonstrated in the previous section, it is compared in this section with state-of-the-art fluids used in commercial high-temperature ORC units. Typically, high-temperature ORC units are fed by a thermal oil heat transfer loop, operating at maximum temperature of 300/310 °C preventing thermal degradation of both the thermal oil itself and the organic fluid. This standard practice is common across various applications such as waste heat recovery (WHR) from electric arc furnaces [50], biomass boiler [5152], CSP, as attested by ORC manufacturers [5354].

However, in recent years, there has been growing interest in direct coupling with the heat source to enhance overall plant efficiency, as the indirect heat coupling limits the potential to cool down the heat source. Moreover, the direct heat transfer solution requires fewer components, reducing system complexity and capital cost. An example of direct heat exchange is Turboden's 0.7 MW_{el} ORC unit, which recovers heat from 400 °C exhaust gases from light fuel oil combustion at a steel rolling mill [55]. Another notable case is the 2 MW_{el} ORC unit installed by Turboden in 2018 at Cementi Rossi (Piacenza, Italy) [56], where direct heat exchange was employed in a cement plant.

In direct heat coupling, even if the working fluid can be operated at turbine inlet temperature considerably lower than the heat source temperature, thermal cracking of the fluid is more likely to occur compared to the thermal oil case. This is primarily due to higher wall temperatures compared to conventional organic fluid-thermal oil heat exchanger, especially at high vapour quality conditions (low heat transfer coefficient). This condition may lead to potential hot spots and fluid degradation, especially within the thermal boundary layer. Therefore, when dealing with heat sources approaching 400 °C, it is preferrable to adopt working fluids with low degradation rates up at 300–350 °C. As a matter of facts, this requirement is met only by few working fluids, such as toluene, cyclopentane, siloxanes, and fluorobenzene. The mentioned fluids are reported in Table 3 along with their key characteristics, thermal stability threshold, and NFPA ratings.

In this section, a typical flue gas from a cement plant is considered as the heat source for evaluating the performance of fluorobenzene as an ORC working fluid. The key characteristics of this flue gas are delineated in Table 4. A flue gas with this characteristics is typical of a cement plant with 2100 tons of clinker per day [64]. Heat recovery from the flue gas is technically possible up to a minimum flue gas temperature of 100 °C, according to the European Cement Research Academy (ECRA) [65]. The

Table 3
Thermal stability threshold of organic fluids for high-temperature ORC and main characteristics.

Fluid	Formula	$T_{stability}$ [°C]	Reference	T_{cr} [°C]	P_{cr} [bar]	NBP [°C]	GWP	ODP	NFPA Health	NFPA Flammability	NFPA Reactivity
Toluene	C_7H_8	400	[45575859]	320	41.1	110.6	3	0	2	3	2
Cyclopentane	C_5H_{10}	350	[3760]	238.6	44.4	49.3	5	0	1	3	1
MM	$C_6H_{18}OSi_2$	300–320	[6162]	246.7	19.4	100.5	n.a.	0	2	4	2
Fluorobenzene	**C_6H_5F**	**350***	**This work**	**287**	**45.5**	**84.7**	**≪1** [30]	**0**	**1** [63]	**3**	**0**

* The investigation in this work extends up to 350°C, revealing low degradation rate.

Table 4
Heat source considered in this work.

Parameters	Value
Temperature [°C]	390
Pressure [bar]	1.0132
Volumetric Flow [m^3/h]	359,000
Minimum temperature [°C]	100
Available Exergy [MW]	8.46
Unavoidable Stack Loss [MW]	0.78
Composition [% mol]	
N_2	67.9
O_2	6.0
CO_2	18.67
H_2O	7.33
NO_2	0.03
SO_2	0.01
CO	0.06

need for a minimum thermal draft in the stack and the risk of corrosion from condensation in filters and stacks restrict the recovery potential, allowing exploitation of exhaust gases only above a temperature threshold of 100 °C. The considerations about the source can be generalized for many other exhaust gases deriving from other industrial applications, such as glass industry o stell mills. The results are, therefore, of general interest.

A recuperated layout of the ORC is considered, according to Fig. 8. The recuperator is important not only to internally recover the heat available at the turbine outlet (increasing the cycle efficiency), but also to increase the temperature of the working fluid at the evaporator – or primary heat exchanger (PHE) – entrance (state "3″): this avoids the cooling of the flue gases below the minimum temperature limitation, in direct heat transfer. The power cycle architecture and a T-s diagram representative of the coupling with the heat source and sink is proposed in Fig. 8. The assumptions adopted to calculate the power cycle conditions are reported in Table 5.

The isentropic efficiency of the turbine is calculated in each operating condition with the correlation developed by Macchi and Astolfi [66] for three-stages axial turbines as function of a size parameter (SP) and the volumetric ratio (V_r). Only subcritical conditions ($P_{eva} < 0.9\ P_{cr}$) are considered as more attaining to commercial ORC units. Both saturated and superheated cycles (with a maximum of 50 °C superheating) have been analysed. Energy and exergy balances are solved in Aspen Plus V12 software using the Peng Robinson EoS in its original form [67]. The main key performance indicators used are the net mechanical power output (W_{net}), the thermal efficiency (η_{th}), and the exergy efficiency (η_{ex}), defined as:

Table 5
ORC modelling assumptions.

Parameters	Values
Minimum Temperature	40 °C
Evaporation Pressure[a]	≤ 0.9 P_{cr}
Degree of Superheating	0–50 °C
ΔT_{min} Recuperator	15 °C
ΔT_{min} PHE	15 °C
Pressure Drop Recuperator (Hot/Cold side)	1 %
Pressure Drop PHE and Condenser	2 %
Cooling Water In/Out Temperature	20/35 °C
Turbine Isentropic Efficiency ($\eta_{is,T}$)	calculated[b]
Pump Isentropic Efficiency ($\eta_{is,P}$)	70 %

[a] optimized;
[b] from 3-stages axial turbine correlation [66] in each design condition

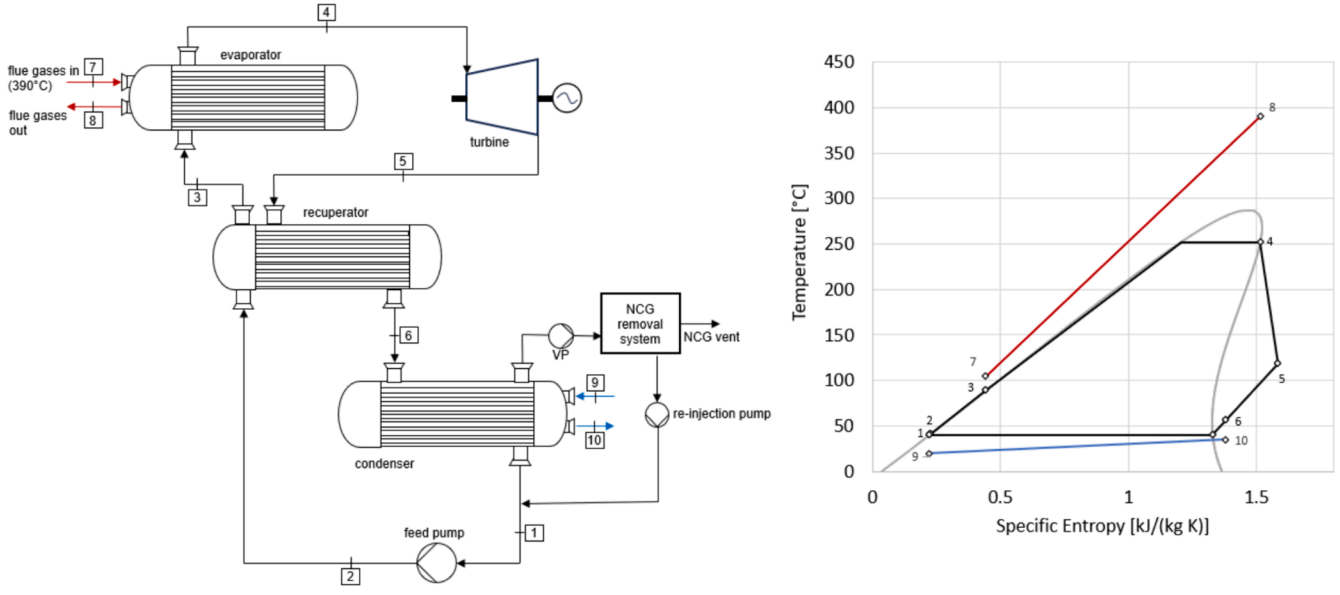

Fig. 8. ORC recuperated cycle layout (left) with direct heat exchange with the flue gases at 390 °C and NCG removal system; T-s diagram of the saturated fluorobenzene cycle at 30 bar evaporation pressure (right).

$$\dot{W}_{net} = \dot{W}_T - \dot{W}_P = \dot{m}_{wf}(h_4 - h_{5,is})\eta_{is,T} - \frac{\dot{m}_{wf}(h_{2,is} - h_1)}{\eta_{is,P}} \quad (3)$$

$$\eta_{th} = \frac{\dot{W}_{net}}{\dot{Q}_{PHE}} \quad (4)$$

$$\eta_{ex} = \frac{\dot{W}_{net}}{\dot{E}x_{source}} = \frac{\dot{W}_{net}}{\dot{m}_{hs} ex_{in}} \quad (5)$$

where $\dot{E}x_{source}$ represents the ideal power that can be extracted from the heat source when it is cooled down to the dead state temperature, i.e. the ambient temperature T_0 (considered 20 °C). The exergy is calculated in each state point according to Equation (6):

$$ex_i = (h_i - h_0) - T_0(s_i - s_0) \quad (6)$$

The exergy balance is computed on each component in order to determine the distribution of the exergy destruction due to irreversibility generation, starting from the available exergy from the source (7.68 MW). An unavoidable exergy loss of 0.78 MW is constituted by the impossibility to cool the heat source down to a temperature lower than 100 °C due to minimum stack temperature imposition (Table 4).

In Fig. 9, the performance an ORC adopting fluorobenzene as working fluid are explored at varying evaporation pressure, considering a direct coupling with the sensible heat source at 390 °C.

Considering subcritical conditions, superheating is not profitable (Fig. 9 – left) as it increases the turbine discharge temperature and, consequently, the temperature of the working fluid at the inlet of the PHE. This decreases the capability to cool the heat source, penalizing the net power production. Considering a saturated cycle configuration, the exergy loss in the PHE reduces when the evaporation pressure increases (Fig. 9 – right) as the temperature profiles of the heat source and the working fluids becomes closer. However, on the other hand, the losses in the turbine increase due to higher volumetric ratio across the turbine, which penalise its isentropic efficiency. Also, the exploitation of the heat source decreases (non-cooling contribution in Fig. 9) at increased evaporation pressure. As a result, there is an optimal evaporation pressure around 30 bar for the saturated cycle (253 °C evaporation temperature), at which point the net produced power is 4.96 MW, resulting in an exergy efficiency of 58.6 %. The T-s diagram in Fig. 8 reports the thermodynamic conditions which optimise the exergy efficiency of the cycle, and associated the state points of the fluorobenzene cycle are reported in Table 6.

The best exergy efficiency condition (evaporating pressure, superheating degree) has been evaluated, in direct exchange with the same heat source at 390 °C, also for the other organic fluids reported in Table 3, for comparison purposes. The results are reported in Table 7.

In direct heat exchange the net power produced, and then the exergy efficiency, of the fluorobenzene cycle is the highest among the fluids considered. The performance of fluorobenzene are similar to those of toluene. The low condensation pressure of toluene, however, results in higher volumetric flow rates at turbine outlet, posing more challenges in the last turbine stages, recuperator, and condenser.

In Table 7 are listed the UA products of the heat exchangers, which provide a comparative indication about the size of the heat exchangers. Regarding the recuperator, the fluids are similar except to the siloxane since its limited temperature drop across the turbine entails large internal heat recovery. The evaporator of the fluorobenzene cycle has similar UA value as the toluene cycle, while it is lower for cyclopentane: the latter has the optimal evaporation pressure near the critical one (at 0.9 P_{cr} as the imposed limit), thus most of the heat is introduced in the cycle at variable temperature determining larger logarithmic mean temperature difference between the source and the working fluid. The siloxane, instead, has low UA value of the PHE as it evaporates at lower temperature, providing large temperature difference with the source.

In case of cyclopentane, even if the saturated cycle provides higher power production, a superheating degree of 11 °C is found to be necessary to avoid excessive cooling of the heat source below the imposed limit of 100 °C. On the contrary, MM is disadvantaged compared to other working fluids in direct exchange due to high molecular complexity entailing a small temperature drop across the

Table 6
Thermodynamic conditions of the fluorobenzene cycle at maximum power production conditions (i.e. maximum η_{ex}); state labels refers to the layout and T-s diagram of Fig. 8.

State Point	T [°C]	P [bar]	ρ [kg/m³]	h [kJ/kg]	s [kJ/kg/K]	x [-]
1	40	0.207	1005.4	455.55	0.221	0
2	41.57	30	1003.5	459.79	0.226	0
3	89.49	29.7	942.3	533.06	0.443	0
4	252.29	29.11	106.4	1035.18	1.513	1
5	118.37	0.213	0.63	892.22	1.582	1
6	56.57	0.211	0.75	818.95	1.379	1

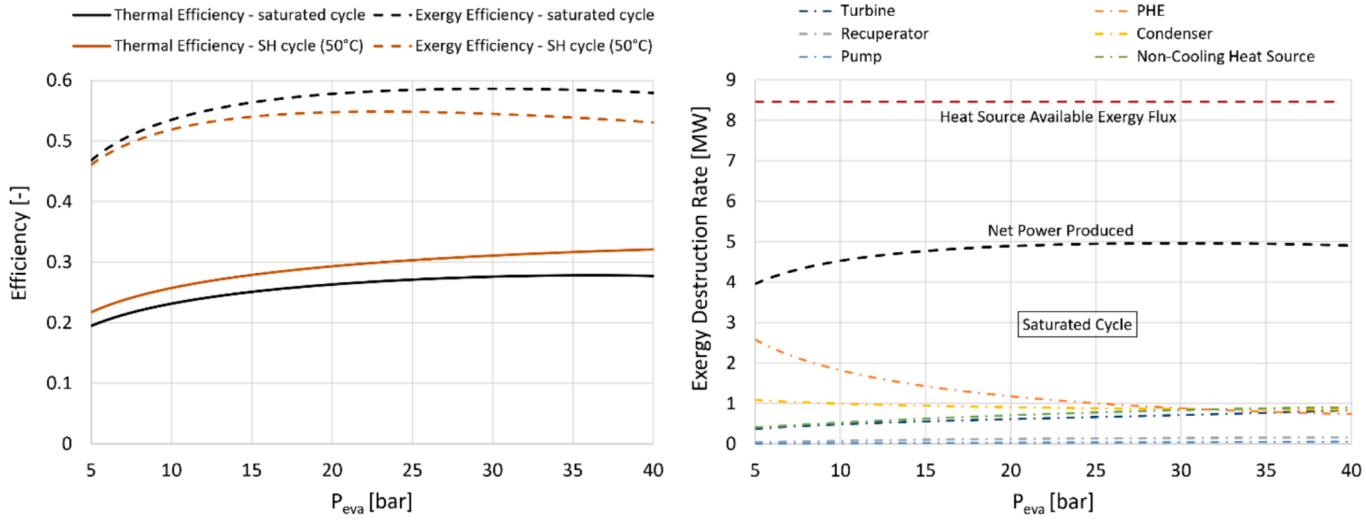

Fig. 9. Fluorobenzene saturated ORC directly coupled with sensible heat source at 390 °C. thermal and exergy efficiency of both saturated and superheated cycle (left); heat source availability, net power production, and exergy destruction in power block components of the saturated cycle (right).

Table 7
Results of ORCs in direct heat exchange with the flue gases detailed in Table 4, at maximum power output condition (best exergy efficiency condition).

Parameter	Fluorobenzene	Toluene	Cyclopentane	MM
η_{ex} [%]	**58.64**	**58.1**	**55.2**	**46.76**
W_{net} [MW]	**4.96**	**4.92**	**4.67**	**3.96**
$\dot{m}_{wf}$ [kg/s]	35.76	30	32.54	49
T_7 [°C]	104.8	114	101	140.1
P_2 [bar]	30	15.5	40.5	12.5
T_{eva} [°C]	253	246	229.5	216
P_{cond} [bar]	0.21	0.08	0.75	0.12
SH Degree [°C]	0	0	11	0
$V_{r,T}$ [-]	159.1	184.3	65.9	141
SP_T [m]	0.36	0.54	0.21	0.53
$\eta_{is,T}$ [%]	84.6	84.3	86.6	85.4
W_T [MW]	5.11	5	4.92	4.07
W_P [MW]	0.15	0.08	0.25	0.12
Q_{PHE} [MW]	17.96	17.4	18.19	15.8
Q_{Rec} [MW]	2.62	3.02	2.72	8.24
Q_{Cond} [MW]	13	12.48	13.52	11.86
UA_{rec} [MW/K]	0.12	0.14	0.13	0.37
UA_{PHE} [MW/K]	0.62	0.65	0.45	0.29
UA_{Cond} [MW/K]	1.1	1.07	1.13	0.96

turbine, and the related incapability to cool the flue gases due to large internal heat recovery (Q_{rec} three times higher than other fluids −Table 7). In Fig. 10, the fractional net power produced, and the exergy losses are reported for the various fluids. It is evident that MM has the highest exergy loss due to non-cooling of the flue gases. For this reason, MM should be considered in a split cycle architecture [51] to reduce the flue gases exhaust temperature. The large exergy losses in the recuperator of MM cycle are due to the highly regenerative nature of the fluid.

4. Fluorobenzene in high-temperature heat pump for 180 °C heat delivery

This section provides a preliminary evaluation of subcritical HTHP performance using fluorobenzene as working fluid, focusing on a heat sink with a constant temperature of 180 °C. The choice of this temperature level aligns with the earlier discussion in the Introduction section, which highlighted the limited availability of fluids suitable for subcritical closed-loop HTHP above 150–160 °C and with the significant industrial heat demand up to 200 °C for steam production. The analysis is extended to other working fluids that can be used in the same application in order to point out the benefits of the proposed solution.

As stated by Angelino and Invernizzi in 1987, ≪*future high temperature fluids are more likely to be found among compounds having a complex molecular structure, recourse to the regenerative cooling of the liquid could become a procedure of general interest*≫ [29]. The molecular complexity of a fluid can be expressed as in Equation (1), and it is proportional to the slope of the saturated vapour curve in the temperature-entropy diagram, measured at a reduced temperature of 0.7:

$$\sigma = \frac{T_{cr}}{R}\left[\frac{ds_{SV}}{dT}\right]_{T_{red}=0.7} \quad (1)$$

The investigated fluids, with critical temperature above 180 °C, are reported in Table 8 along with their main characteristics such as the normal boiling point (NBP), the acentric factor (ω), the molecular complexity (σ) and the critical parameters (T_{cr}, P_{cr}).. The thermodynamic properties are taken from Aspen Plus V12 [68].

The saturation curves of the working fluids are reported in Fig. 11 in the P-h diagram.

The key performance parameter of the HTHP is measured by the coefficient of performance (COP), which describes the ratio between supplied heat ($\dot{Q}_{sink}$) at the condenser and consumed power by the compressor ($\dot{W}_{comp}$):

$$COP = \frac{\dot{Q}_{sink}}{\dot{W}_{comp}} \quad (2)$$

The constraints and assumptions of the analysis are reported in Table 9. A maximum lift of 100 °C (difference between T_{cond} and T_{eva}) is considered, as it approaches the practical threshold for a two-stage centrifugal compressor. This limit is reached due to excessively high pressure ratios for the majority of refrigerants [69]. Then, the evaporation temperature is limited above 70 °C, and the HTHP is considered to be thermally integrated with low-grade waste heat to be valorised (such as flue gases before stack). An isentropic efficiency of 75 % is assumed for the compression step to allow a fair comparison among different working fluids, as in Abedini et al. [28]. Most of the correlations available in the literature are for volumetric compressors, while the focus here is on MW-scale industrial heat pumps, where centrifugal compressors are more likely to be adopted. However, in Appendix C, results including the screw compressor efficiency of Ganesan and Eikevik [70] are presented, valuable for kW-scale HTHP. The pressure losses in the heat exchanger are neglected. The Peng Robinson EoS [67] is used in Aspen Plus V12, with the parameters in Table 8, to calculate the thermodynamic properties of the fluids and for the optimisation of the HTHP.

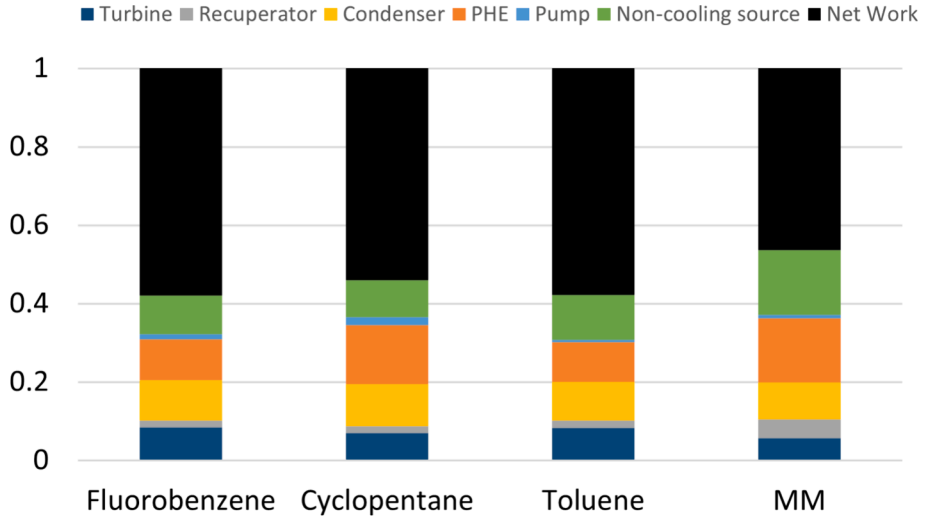

Fig. 10. Fraction of net power produced and exergy losses in each component starting from the available exergy of the flue gases.

Table 8
Main characteristics of fluorobenzene and other low-GWP fluids potentially suitable for subcritical HTHP at 180 °C sink temperature.

Compound	Formula	MW [g/mol]	σ [-]	T_{cr} [°C]	P_{cr} [bar]	ω [-]	NBP [°C]	P_{sat} at 180 °C [bar]
Fluorobenzene	**C_6H_5F**	**96.1**	**0.69**	**287**	**45.5**	**0.247**	**84.7**	**9.4**
Cyclopentane	C_5H_{10}	70.1	0.75	238.6	45.1	0.195	49.2	19.5
n-Pentane (R601)	C_5H_{12}	72.2	1.4	196.6	33.7	0.252	36.1	26.3
Cyclohexane	C_6H_{12}	86.2	1.42	280.7	40.8	0.208	80.7	9.4
Hexane	C_6H_{14}	86.2	1.71	234.5	30.3	0.301	68.7	13
Heptane	C_7H_{16}	100.2	1.84	267.1	27.4	0.349	98.4	6.9
Acetone	C_3H_6O	58.1	−0.2	235	47	0.307	56.1	19.9
Butanol	$C_4H_{10}O$	74.1	0.83	290	44.1	0.588	118.8	5.9
Ethanol	C_2H_6O	46.1	−3.14	240.9	61.4	0.644	78.3	19.7
Methanol	CH_3OH	32	−10.1	239.4	80.8	0.566	64.7	27.8

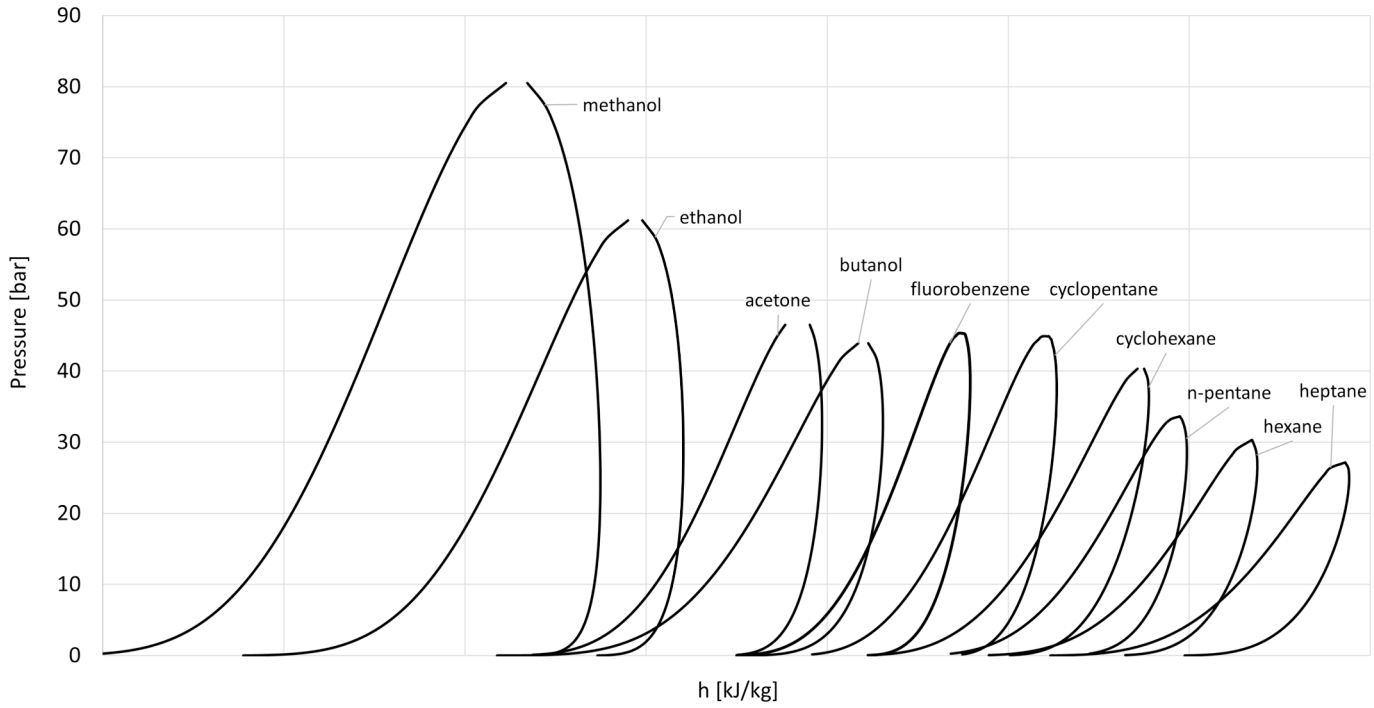

Fig. 11. Saturation curves of the working fluids considered for the subcritical HTHP in the pressure-specific enthalpy diagram.

Table 9
HTHP modelling assumptions.

Parameters	Values
Evaporation Temperature	70–130 °C
Condensation Temperature	180 °C
ΔT_{min} IHX	10 °C
ΔP Heat Exchangers	neglected
Compression Isentropic Efficiency ($\eta_{is,C}$)	75 %
ΔT_{SH} at Compressor Inlet*	≥ 2 °C

* In regenerative cycles, the IHX should provide a proper degree of superheating to avoid condensation in the compressor.

As reported in Table 9, a minimum of 2 °C of superheating at compressor inlet is assumed (for non-regenerated cycles). However, given the high critical temperature fluids considered in this analysis, the adoption of an internal heat exchanger (IHX) recuperator is necessary to provide an adequate degree of superheating at compressor inlet, which allows to avoid two-phase conditions inside the compressor [8]. Regeneration is necessary in case of complex fluid (elevate number of atoms in the molecule) possessing retrograde dew curve in the P-h diagram (Fig. 11), such as most of high-critical temperature fluids. Therefore, the performance of the cycle improves and condensation within the compressors is prevented.

The IHX has negative impacts on fluids with low molecular complexity, resulting in: i) high temperature at compressor outlet due to low heat capacity; ii) associated risk of fluid thermal cracking; and iii) increased chances of compressor failure.

The regenerated HTHP architectures considered in this analysis are represented in Fig. 12: a) one-stage throttling cycle; b) two-stage throttling cycle with regeneration in the lower portion of the cycle. In cycle (a), regeneration is carried out by subcooling the liquid at condenser outlet; in cycle (b), regeneration is performed between the vapour exhausted by the evaporator and the liquid before the last throttling, flashed at an intermediate pressure (P_{int}). The vapour compressed in the low pressure (LP) compressor of the HTHP type (b) is mixed with the vapour flashed at the same pressure: as a result, it is evident in Fig. 12, that the discharge temperature after the high-pressure (HP) compression step is lower for cycle (b) at the same ΔT_{min} of the recuperator (IHX). The portion of the regenerative sub-cycle is determined by the intermediate pressure, which is determined through a proper optimization procedure for each fluid and temperature lift. Similar cycle architecture was also considered by Dong et al. [71].

The thermodynamic conditions of the fluorobenzene HTHP, according to the cycle architectures presented in Fig. 12, are reported in

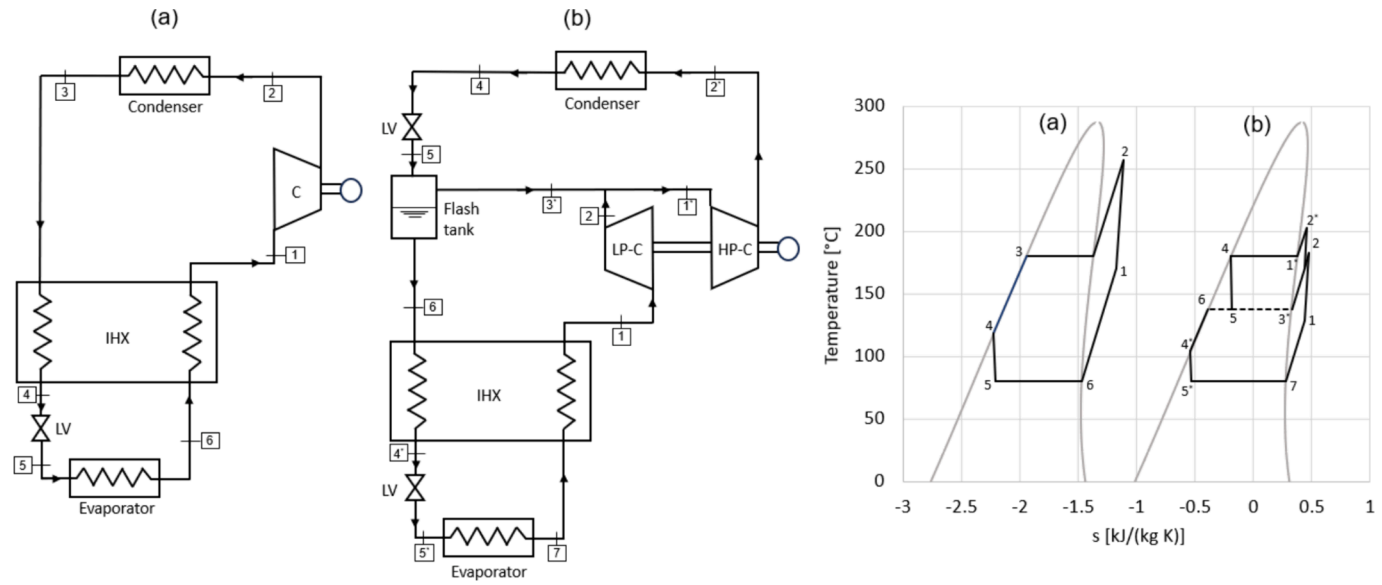

Fig. 12. Cycle architectures adopted for the subcritical 180 °C HTHP; a) regenerative cycle with one-stage throttling; b) two-stage throttling with regeneration in the low-temperature portion; T-s diagram of the corresponding cycles using fluorobenzene at 100 °C temperature lift at best COP conditions.

Table 10
Thermodynamic conditions of the fluorobenzene HTHP at 180 °C delivery and 100 °C temperature lift in configurations (a): state labels refers to the layout and T-s diagram of Fig. 12.

State Point	T [°C]	P [bar]	ρ [kg/m³]	h [kJ/kg]	s [kJ/kg/K]	x [-]
1	170	0.87	2.3	962.3	1.629	1
2	256.7	9.36	22.6	1088	1.691	1
3	180	9.36	802.3	700	0.857	0
4	118.4	9.36	917.2	581.2	0.576	0
5	80	0.87	14.6	581.2	0.588	0.2
6	80	0.87	2.9	843.5	1.331	1

Table 11
Thermodynamic conditions of the fluorobenzene HTHP at 180 °C delivery and 100 °C temperature lift in configuration (b): state labels refers to the layout and T-s diagram of Fig. 12.

State Point	T [°C]	P [bar]	ρ [kg/m³]	h [kJ/kg]	s [kJ/kg/K]	x [-]
1	127.8	0.87	2.6	903.2	1.489	1
2	182.1	4	10.9	974.5	1.529	1
1*	169.9	4	11.2	956	1.487	1
2*	202.5	9.36	26.4	996.1	1.509	1
3*	137.8	4	12.3	909.8	1.379	1
4	180	9.36	802.3	700	0.857	0
5	137.8	4	41.8	700	0.868	0.29
6	137.8	4	883.8	616.1	0.665	0
4*	104.3	4	936.6	556.5	0.513	0
5*	80	0.87	23.3	556.5	0.518	0.12
7	80	0.87	2.9	843.5	1.331	1

Table 10 and Table 11 for 100 °C temperature lift (evaporation temperature of 80 °C).

It is important to emphasize that, in cycle (a), the reduction of the compressor discharge temperature can be only achieved by decreasing the design effectiveness of the recuperator (IHX). In general, the presence of an internal heat exchanger (IHX) increases the compressor discharge temperature, and there is a risk of thermal cracking for some fluids above 200 °C. Furthermore, high discharge temperatures pose additional challenges in compressor design, although these aspects are beyond outside the scope of the present study.

The influence of recuperator size (ΔT_{min} in the IHX) on the COP and compressor discharge temperature in a one-stage throttling cycle ("a" in Fig. 12) operating with fluorobenzene at 100 °C temperature lift is illustrated in Fig. 13. At 100 °C lift, a minimum superheat (SH) of 21 °C is necessary for fluorobenzene to prevent condensation in the compressor in a one-stage throttling cycle.

(SH) necessary at the compressor inlet for various working fluids in a one-stage throttling cycle is illustrated in Fig. 14. Acetone, methanol, and ethanol are not included in Fig. 14 as they do not present condensation issues in the compressor, being the least complex fluids considered (the only fluids with negative complexity in Table 8).

It is evident that highly complex fluids such as heptane, hexane, and cyclohexane (with a pronounced retrograde saturation curve in P-h diagram) inherently requires a significant degree of superheating at compressor inlet. Therefore, a large recuperator is necessary to prevent the occurrence of a two-phase region during the compression step in single-stage throttling cycle.

The COP of the different potential working fluids delivering 180 °C heat in single-stage throttling HTHP is reported in Table 12, considering a temperature lift of 100 °C.

Fluorobenzene demonstrates the highest COP (3.09) at a 100 °C lift, closely followed by cyclohexane (3.08) and butanol (3.06). Notably, fluids with higher critical temperature (Table 8) exhibit superior COP. Conversely, the lower performance of n-pentane cycle (COP of 2.55) can be attributed to its condensation temperature approaching the critical point, resulting in operation within an unfavourable reduced temperature region. For methanol, the least complex fluid (σ = -10.1), regeneration adversely affects the COP in single-stage throttling cycle, leading to the exclusion of the IHX recuperator (2 °C of superheating assumed at compressor inlet).

It should be noted that not only the COP, but also other factors affect the feasibility of a HTHP delivering heat at 180 °C. The thermo-chemical integrity of the working fluid is a key factor to be considered, expect for working fluids with demonstrated stability at 300 °C or above such as n-pentane and cyclopentane [45]. For instance, the butanol cycle's compressor discharge temperature is around 277 °C if the IHX recuperator is operated with a 10 °C pinch point. However, thermal decomposition of butanol is not negligible even at 220 °C, as determined by our previous experimental campaign [46]. The same thermal stability is expected for other alcohols such as ethanol and methanol having the bonds in the alkyl chain. Therefore, a smaller recuperator should be

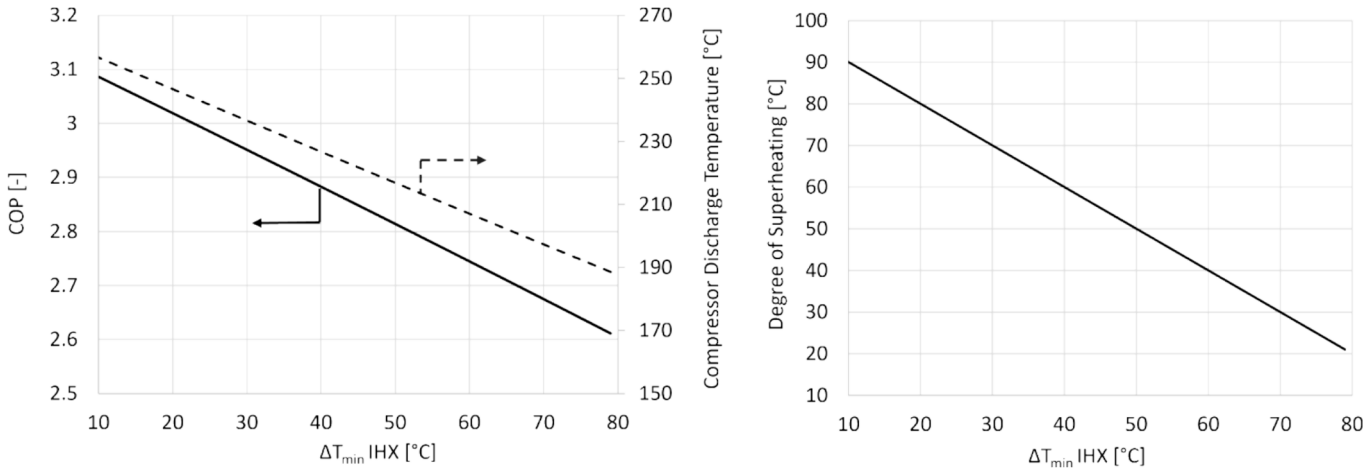

Fig. 13. Fluorobenzene HTHP one-stage throttling (type a) at 180 °C condensation and 100 °C lift (80 °C evaporation). on the left, the impact of regeneration on the COP and compressor discharge temperature; on the right, the relation between ΔTmin in the IHX recuperator and the resulting degree of superheating at compressor inlet.

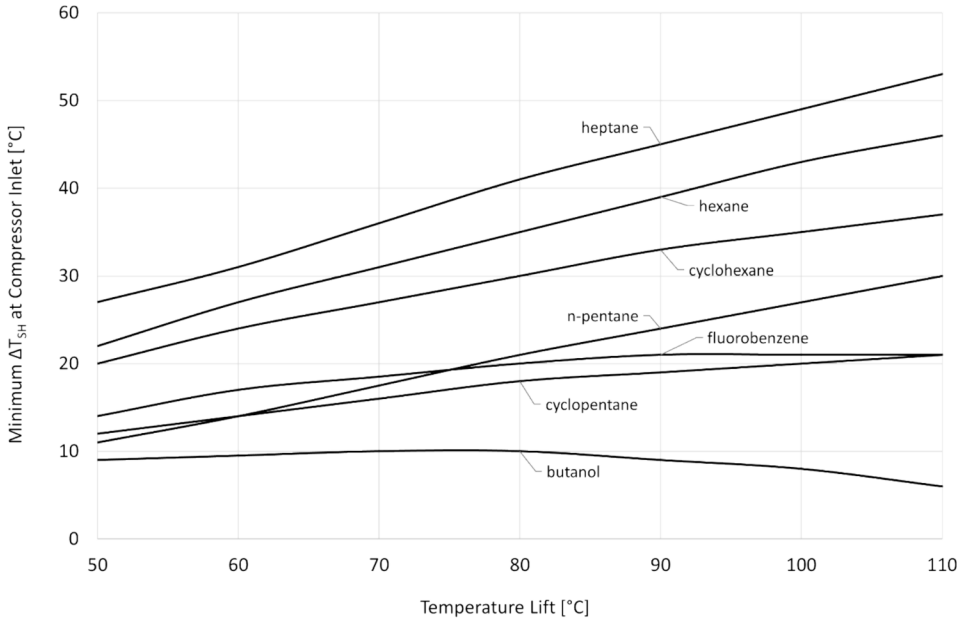

Fig. 14. Minimum Degree of Superheating requirements at compressor inlet for different working fluids in one-stage throttling HTHP, at 180 °C condensing temperature, as function of temperature lift; methanol, ethanol and acetone do not face two-phase compression issues.

Table 12
Results of subcritical HTHP at 180 °C condensing temperature and 80 °C evaporation temperature (100 °C lift), in one-stage throttling (Fig. 12-a).

Fluids	COP	ΔT_{min} IHX [°C]	Compressor Discharge T [°C]	Risk of thermal cracking?	Δh_{comp} [kJ/kg]	Δh_{cond} [kJ/kg]	Δh_{eva} [kJ/kg]	Δh_{IHX} [kJ/kg]	$\dot{Q}_{IHX}/\dot{Q}_{cond}$
Fluorobenzene	**3.09**	**10**	**256.6**	**No**	**125.7**	**388**	**262.3**	**119**	**0.31**
Cyclopentane	2.92	10	252	**No**	141.8	414.3	272.4	153.9	0.37
Acetone	2.87	10	287.8	**n.a.**	197.6	566.7	369.1	150.1	0.26
Ethanol	2.81	10	341.1	**Yes**	342.4	961.4	619.1	160.4	0.17
Methanol*	2.73	–	328.8	**Yes**	407.2	1109.2	702.1	–	–
Butanol	3.06	10	277.2	**Yes**	224.4	685.9	461.5	168.2	0.25
Hexane	2.9	10	231.3	**n.a.**	122.5	354.8	232.3	191.4	0.54
Heptane	3.03	10	226.9	**n.a.**	121.5	368.1	246.6	190.1	0.52
n-Pentane	2.55	10	238.8	**No**	124.5	317.2	192.6	194.3	0.61
Cyclohexane	3.08	10	240.7	**n.a.**	134.1	413.5	279.4	158.7	0.38

* No IHX recuperator is used for this fluid as it has a negative impact on COP, and 2 °C of superheating at evaporator outlet is assumed; n.a. stands for "not available" information about thermal stability.

Table 13
Results of subcritical HTHP at 180 °C condensing temperature and 80 °C evaporation temperature (100 °C lift), in two-stage throttling (Fig. 12-b).

Fluids	COP	$P_{int,opt}$ [bar]	ΔT_{min} IHX [°C]	Compressor Discharge T [°C]	Risk of thermal cracking?	$\dot{m}_{LP}/\dot{m}_{HP}$ [-]	$\Delta h_{comp,LP}$ [kJ/kg]	$\Delta h_{comp,HP}$ [kJ/kg]	Δh_{cond} [kJ/kg]	Δh_{eva} [kJ/kg]	Δh_{IHX} [kJ/kg]	$\dot{Q}_{IHX}/\dot{Q}_{cond}$
Fluorobenzene	**3.25**	**4**	**10**	**202.5**	**No**	**0.72**	**71.4**	**40.1**	**296.4**	**287.3**	**59.9**	**0.14**
Cyclopentane	3.1	9.5	10	198	**No**	0.64	81.4	41.6	289.9	308.5	77.5	0.17
Acetone	3.14	9	10	226.2	**n.a.**	0.7	111.1	60.8	433.6	422	77.2	0.13
Ethanol*	3.12	6.5	–	235.7	**Yes**	0.74	156.7	111.1	707	653	–	–
Methanol*	3.05	9.5	–	308	**Yes**	0.77	220.2	177	1062	929	–	–
Butanol	3.27	2	10	219.4	**Yes**	0.75	129.4	70.9	551	508.5	85.9	0.12
Hexane	3.06	7	10	185.9	**n.a.**	0.6	80.5	28.3	234.3	262.4	115	0.29
Heptane	3.15	3.5	10	183.1	**n.a.**	0.65	81	28.6	257.2	268	114.1	0.29
n-Pentane	2.79	16	10	192.1	**No**	0.48	85.4	23.2	179.8	239.5	125.9	0.34
Cyclohexane	3.21	4.5	10	191	**n.a.**	0.69	80.3	38.4	301.5	302.5	83.5	0.19

* No IHX recuperator is used for this fluid as it has a negative impact on COP, and 2 °C of superheating at evaporator outlet is assumed.

adopted for butanol, resulting in reduced COP and compressor discharge temperature as a consequence. Similar thermal stability is expected for ethanol and methanol, given the similar molecular structure. For this reason, the feasibility of a fluid in HTHP delivering 180 °C heat is assigned in Table 12 and Table 13 also by indicating whether thermal cracking of the organic fluid is likely to occur. In case of methanol, even although no IHX recuperator has been adopted due to its detrimental effect on COP, the low molecular complexity (σ = -10.1) results in high compressor overheating, likely exceeding the thermal stability limit. Consequently, methanol is deemed unsuitable for use in a single-stage throttling HTHP at the conditions explored in this work.

As a matter of facts, fluorobenzene and cyclohexane emerge as the most promising candidates for single-stage throttling HTHP at 180 °C condensing temperature. Cyclohexane's high molecular complexity (σ = 1.41) provides high vapour heat capacity, preventing compressor overheating and consequent superheating losses. However, the downside of cyclohexane's complexity is the need for significant degree of superheating at compressor inlet (refer to Fig. 14) to avoid condensation within the compressor, posing challenges if the recuperator effectiveness decreases during off-design. On the other hand, fluorobenzene, with a moderate molecular complexity (σ = 0.69), experiences more overheating in the compressor but requires fewer regeneration to avoid critical two-phase zones.

By adopting a two-stage throttling (cycle type "b" in Fig. 12), a greater flexibility is introduced to optimise the cycle, primarily through the flash intermediate pressure (first throttling discharge pressure). This pressure level determines the portion of the sub-cycle with regeneration on the overall cycle, as well as the mass flow rates in the upper and lower sub-cycles. The low-pressure compressor (1–2 in Fig. 12-b) elaborates lower mass flow rate than the high-pressure compressor (1*-2* in Fig. 12-b), depending on the mass vapour quality of the state point 5 (Fig. 12– b) after the first throttling valve. The results of the different working fluid in two-stage-throttling architecture at 180 °C delivery and 100 °C temperature lift are presented in Table 13.

In comparison to the one-stage throttling cycle results, the HTHP with two-stage throttling demonstrates the potential for lower compressor discharge temperature and higher COP values. The ratio of the IHX thermal power to the delivered power at the condenser is lower in this case, as regeneration occurs only in the low-temperature sub-cycle. The mixing of flashed vapour with the vapour discharged by the low-pressure compressor reduces the compression work of the high-pressure compression stage. Fluids characterized by low heat capacity

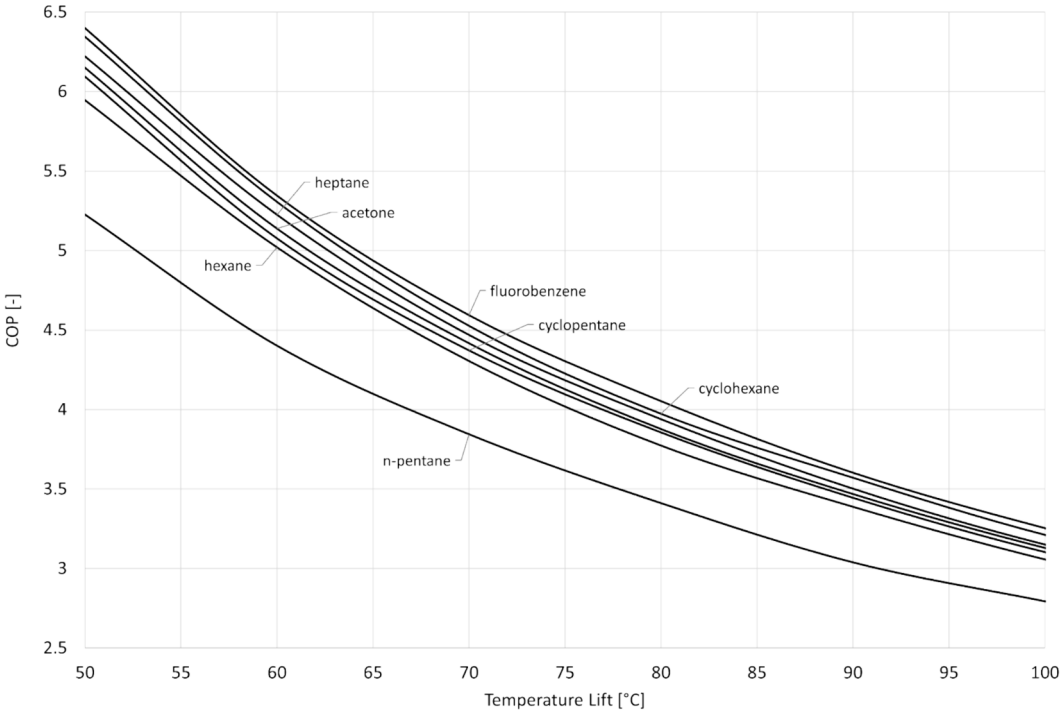

Fig. 15. COP of subcritical HTHP with different working fluids condensing at 180 °C at varying temperature lift, in two-stage throttling architecture (Fig. 12-b).

(molecular complexity), such as ethanol and methanol, the regenerative IHX has a detrimental effect on the performance and is therefore excluded from the analysis. This is because fluids with fewer internal degrees of freedom can only transfer additional energy input as translational movement, while complex fluids can distribute most of the energy across rotational and oscillating degree of freedom.

Among the considered fluids, butanol achieves the highest COP (3.27) in this cycle configuration. However, the compressor discharge temperature reaches approximately 220 °C, leading to non-negligible thermal cracking of the fluid, then raising doubts about the feasibility of a butanol cycle under these conditions. Fluorobenzene follows closely with the second highest COP value (3.25). Cyclohexane has similar COP value (3.21), but the operability range of this fluid is very limited by the high molecular complexity of the fluid, which requires a ΔT_{min} of the IHX lower than 20 °C (equivalent to a minimum superheating degree at LP compressor inlet of 42 °C) to avoid condensation in the compressor. Consequently, there is high risk of compromising the compressor if the IHX recuperator effectiveness decreases during off-design conditions. In contrast, fluorobenzene does not encounter such limitations, as the ΔT_{min} of the IHX can increase up to 44 °C without incurring two-phase compression. Given this feature and the high COP value (3.25) at 100 °C lift, fluorobenzene emerges as a promising candidate for this application. The working fluids are compared in Appendix C, at 100 °C temperature lift, also including a correlation for the compressor isentropic efficiency.

In the end, the results of different working fluids in the two-stage throttling HTHP cycle layout are represented in Fig. 15 at varying temperature lift; the cycles are properly optimised in each condition. Ethanol, methanol, and butanol are omitted from Fig. 15 as their compressor discharge temperature is excessive, as discussed, and are impractical for 180 °C condensation temperature.

In conclusion, fluorobenzene represents one of the most interesting working fluids, combining high COP values, no strict requirements for regeneration to avoid two-phase compression compared to more complex fluids (cyclohexane, hexane, heptane), good thermo-chemical stability as demonstrated in the previous section, and high auto-ignition temperature (455 °C).

5. Conclusion

Fluorobenzene is proposed for the first time as versatile working fluid for both Organic Rankine Cycles (ORC) and High-Temperature Heat Pumps (HTHP). The fluid possesses near zero GWP, zero ODP, and relatively low cost, and low toxicity compared to benzene. Moreover, fluorobenzene is not classifiable as PFAS substance, which are undergoing strict regulation in EU.

The thermo-chemical stability of fluorobenzene is experimentally tested in this study with a consolidated procedure in the Fluid Test Laboratory of the University of Brescia. Compared to past studies, the well-established static thermal stability method has been included in a broader framework in this work. The presence of a non-condensable-gases (NCG) removal system in commercial ORC has been simulated during the experimental campaign. The effect of time on the unimolecular decomposition reaction of the fluid has been assessed at constant temperature (350 °C). As a result of the investigation, all degradation products appear in the vapour phase: after a brief aspiration of the fluid post thermal stress, the volumetric behaviour of the thermally-stressed fluorobenzene up to 350 °C returned the reference behaviour of the fresh fluid. This result proves that, after aspiration of fluorobenzene in the hot-well of an ORC and the subsequent NCGs removal, the fluid recovered in the gas treatment unit and recirculated in the system maintains its physical properties unaltered. These results have been obtained not only by measuring the volumetric behaviour in laboratory, but also by a chemical analysis on the thermally-stressed fluid (after the thermal stability campaign) after prolonged thermal exposure at 350 °C. The FTIR analysis on the liquid confirms that no substantial traces of any other degradation compound in the liquid phase.

The small degradation rate at 350 °C poses fluorobenzene among the most thermally stable organic fluids, comparable with toluene and cyclopentane, adopted in high-temperature ORC units. Given the good thermal stability, fluorobenzene has been studied in direct heat exchange with a medium–high temperature source. In particular, flue gases available at 390 °C have been considered. From 8.5 MW ideally available as exergy flux of the sensible heat source, the fluorobenzene cycle can produce about 5 MW as mechanical power output, reaching 58.6 % exergy efficiency. The net power production of fluorobenzene surpasses that of other high-temperature ORC working fluids, although the production of toluene cycle is similar.

In high-temperature heat pump (HTHP) application, the performance of fluorobenzene have been studied in case of 180 °C as heat delivery temperature, given the literature gap for subcritical heat pumps above 150/160 °C. A cycle architecture with internal heat exchanger was found necessary to avoid two-phase states during the compression of the fluid, as it is for most of the high-critical temperature fluids considered in this study. The Coefficient of Performance of the fluorobenzene HTHP at 100 °C temperature lift is 3.09 in one-stage throttling cycle and 3.25 in two-stage throttling architecture. Considering the efficiency of the compressor as a function of operating conditions (Appendix C), fluorobenzene emerges as the most efficient working fluid among those investigated. From this preliminary thermodynamic analysis, fluorobenzene represents one of the most promising working fluids for HTHP covering the heat demand in the temperature range near 200 °C. In fact, as discussed in this article, fluorobenzene not only presents elevate COP values, but also it has no strict requirements for regeneration to avoid two-phase compression compared to more complex fluids (cyclohexane, hexane, heptane), good thermo-chemical stability (as experimentally demonstrated), high critical temperature, and high auto-ignition temperature (455 °C).

CRediT authorship contribution statement

M. Doninelli: Writing – original draft, Visualization, Validation, Software, Resources, Methodology, Investigation, Formal analysis, Data curation, Conceptualization. **G. Di Marcoberardino:** Writing – review & editing, Supervision, Methodology. **I. Alessandri:** Writing – review & editing, Validation, Investigation. **C.M. Invernizzi:** Writing – review & editing, Methodology. **P. Iora:** Writing – review & editing, Supervision, Project administration, Funding acquisition.

Declaration of competing interest

The authors declare that they have no known competing financial interests or personal relationships that could have appeared to influence the work reported in this paper.

Data availability

Data will be made available on request.

Acknowledgements

The research is partly funded by the project HICLOPS “High-medium temperature closed power cycles for waste heat recovery and renewable sources” - under the MUR Progetti di Rilevante Interesse Nazionale (PRIN) Bando 2022 under grant No 2022HMZ39A.

The research is also partly funded by the project "COFFEE" under the National Recovery and Resilience Plan (PNRR), Mission 4 Component 2 Investment 1.3, Project title "Network 4 Energy Sustainable Transition – NEST" funded by the European Union – NextGenerationEU (Project Code PE0000021), Cascade call of the Spoke 5 "Energy Conversion".

The authors thank the Department of Translational Medicine of the University of Brescia for providing the access to the ATR.

Appendix A. – Uncertainty of the experimental results

The global uncertainty of the experimental vapour pressures measured during the thermal stability test are here reported. The total uncertainty of the pressure u_P values is computed according to equation A(1):

$$u_P = \sqrt{(\sigma_P)^2 + (u_{instrumental})^2} \tag{A1}$$

where σ_P is the standard deviations of the measured pressure over 15 min recording with 180 sampling, and $u_{instrumental}$ is the contribution related to the accuracy of the pressure transmitter (in Table 1). The pressure transmitter has been operated at 1 bar full scale, and the resulting accuracy is 1 mbar.

The uncertainty related to each vapour pressure measurement presented in Fig. 3 (stage 1) and 4 (stage 2) are reported below in Figs. F1 and F2.

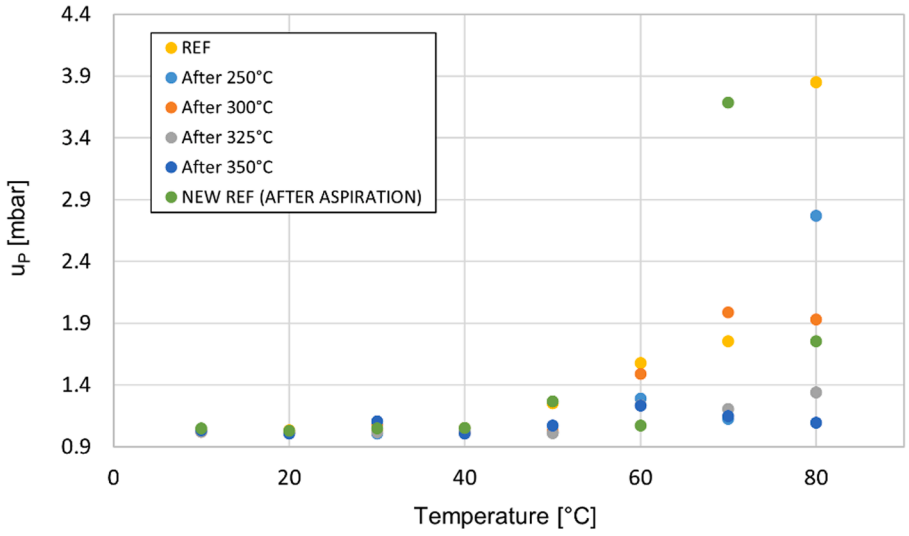

Fig. F1. Uncertainty of the vapour pressures measured during the 1st stage of experimental campaign (refer to Fig. 3).

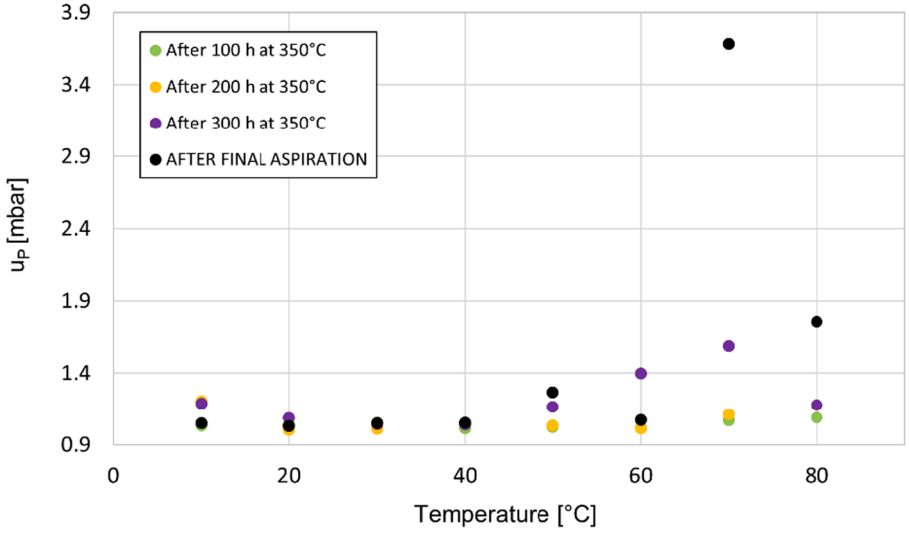

Fig. F2. Uncertainty of the vapour pressures measured during the 2st stage of experimental campaign (refer to Fig. 4).

Appendix B. – Rate of unimolecular decomposition k* (new vs old approach)

The methodology adopted to calculate the quasi-constant rate of decomposition k* of a working fluid, following thermal stability test, is detailed in this section. Moreover, the main methodological differences between the approach adopted in this work and that used in past literature works are here described.

The equations (1–8) presented in a previous literature work [45] are used in this research, but with different approach. The main equations used for the calculation of k* are reported below for clarity purposes; please refer to the reference and nomenclature for the description of each term.

$$\frac{\ln(1-\overline{\beta})}{\Delta t} = -k^* \tag{A2}$$

$$\overline{\beta} = \frac{1}{N}\sum_{i=1}^{N}\frac{\Delta P_{v,i}}{P_{ref,i}}\frac{P_{vr,i}}{T_{vr,i}}z_{cr} \tag{A3}$$

As described in Equations A(2) and A(3), the k* is retrieved from the calculation of the term $\overline{\beta}$, that is proportional to the average value (over the N data points where the vapour pressure is calculated) of each vapour pressure deviations ($\Delta P_{v,i}$) against the reference vapour pressure at the same temperature ($P_{v,i}$). Fig. F3 illustrates the conceptual difference between this work and the previous literature works dealing with the calculation of k*: the pressure deviations resulting from a constant-temperature thermal stress are measured from the previous vapour pressure measured after the previous thermal stress. Instead, in previous works, the pressure deviations were calculated from the reference (fresh fluid) behaviour.

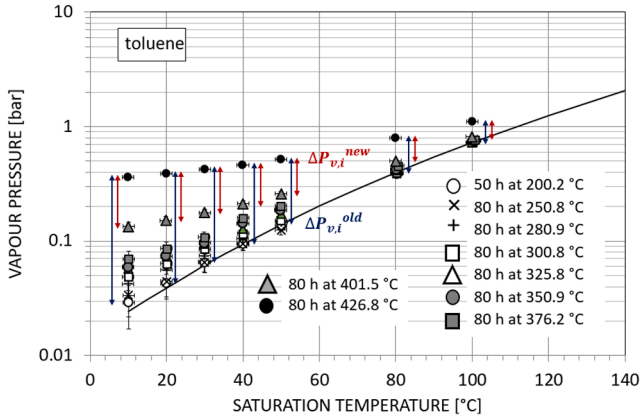

Fig. F3. Example of ΔPv,i (Eq. A(2) measurements for the calculation of k* at 427 °C for toluene [45] with new approach compared to the old one. the vapour pressure increase resulting from a constant-temperature thermal stress is measured excluding the formation of degradation products due to preceding thermal stresses at lower temperatures

This conceptual shift, represented in Fig. F3, has been considered as the formation of degradation products at a certain temperature is noticeable as a pressure increase compared to the vapour pressure measured before thermal stress. Then, the ($\Delta P_{v,i}$) arising from previous thermal stresses at lower temperatures are not accounted for the calculation of k* at a certain temperature: those $\Delta P_{v,i}$ must be allocated to the degradation occurring at lower temperatures.

From a qualitative standpoint, this new approach does not preclude the results described in previous works. The qualitative trend of k* does not change with methodology, as demonstrated in Fig. F4 for toluene. In fact, when approaching temperatures at which fluid decomposition is relevant (above 400 °C in Fig. F3), the vapour pressure variations $\Delta P_{v,i}$ become high both considering as reference ($P_{rev,i}$) the vapour pressure measured after previous thermal stress (at lower temperature) or the fresh fluid vapour pressure (see Fig. F3). The qualitative coherence is presented also in Fig. F4: both approaches identifies a rapid increase of toluene degradation starting from temperatures above 370–390 °C.

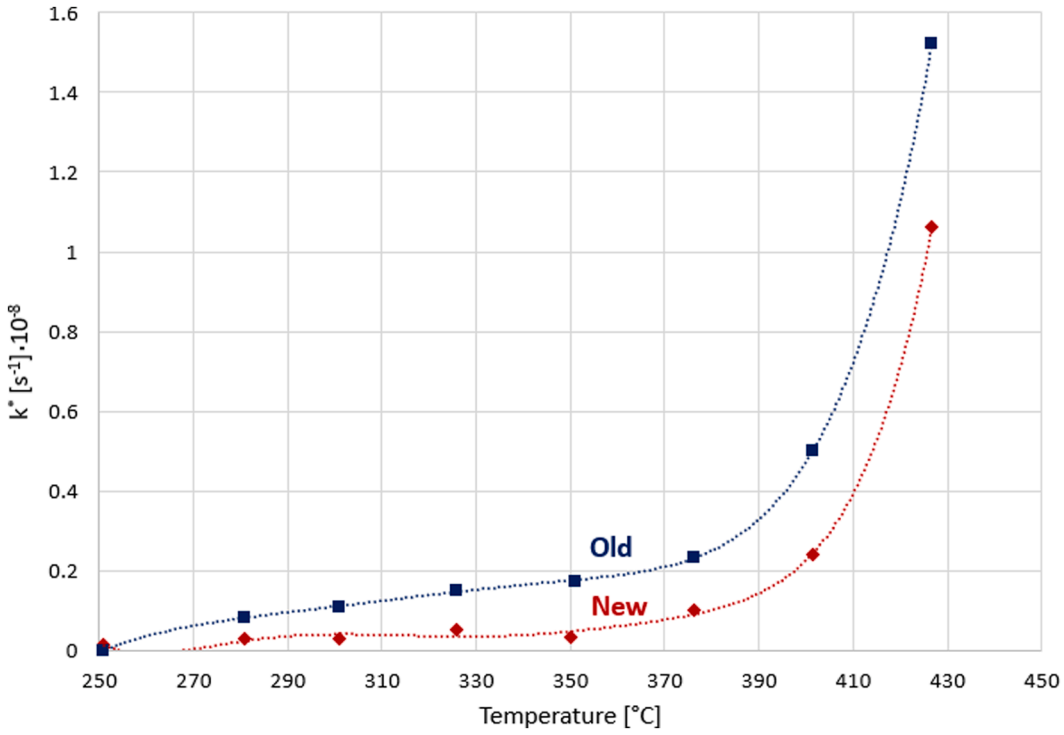

Fig. F4. Resulting k* of toluene test [45] from the new approach adopted in this work and the previous one – the qualitative trend of fluid degradation is not affected by the methodology as the k* rapidly increases in the same temperature range (370–390 °C).

Appendix C. – HTHP results including compressor efficiency correlation

From the results of Section 4, it is evident that the most promising HTHP cycle configuration is the two-stage throttling cycle with regenerative cooling of the flashed liquid (Fig. 12-b), at high temperature lift. The performance of such configurations are reevaluated in this Section introducing one major difference compared to the assumptions in Table 7: the compressors isentropic efficiency is not kept as a constant value, but a correlation is used. The correlation of Ganesan and Eikevik [70], as in Eq. A(4), is used to determine the compressor isentropic efficiency as function of the pressure ratio:

$$\eta_{is,C} = -0.00000461x^6 + 0.00027131x^5 - 0.00628605x^4 + 0.07370258x^3 - 0.46054399x^2 + 1.40653347x - 0.87811477 \quad \text{(A4)}$$

where x is the pressure ratio across the single compressor. The volumetric efficiency of the compressor is fixed at the value 1 instead. The same approach has been adopted by Špale et al. [72] for the screening of different working fluids for a 100 kW high-temperature heat pump.

It must be noted that the correlation in Eq. A(4) is representative of a screw compressor, thus valuable for applications where the compressor consumption does not exceed around 500 kW. The results in Section 4 are, instead, more representative of MW-scale industrial heat pumps adopting centrifugal compressors: the total pressure ratio can be spitted in several stages maintaining good efficiency at values in the 75–85 % range [69].

The calculations here presented focus on a temperature lift of 100 °C, i.e. the evaporation temperature of the working fluid is 80 °C and the condensation temperature is kept 180 °C. This allows a direct comparison with the previous results – with fixed compressor efficiency – of Table 13. These conditions are representative of the upgrading of waste heat or district heating network. The results are presented in Table T1.

Table T1
Results of subcritical HTHP at 180 °C condensing temperature and 80 °C evaporation temperature (100 °C lift), in two-stage throttling (Fig. 12-b) considering the compressor isentropic efficiency as in Eq. A(4).

Fluids	COP	$P_{int,opt}$ [bar]	ΔT_{min} IHX [°C]	Compressor Discharge T [°C]	Risk of thermal cracking?	$\dot{m}_{LP}/\dot{m}_{HP}$ [-]	$\Delta h_{comp,LP}$ [kJ/kg]	$\Delta h_{comp,HP}$ [kJ/kg]	Δh_{cond} [kJ/kg]	Δh_{eva} [kJ/kg]	Δh_{IHX} [kJ/kg]	$\dot{Q}_{IHX}/\dot{Q}_{cond}$
Fluorobenzene	**3.17**	**3**	**10**	**191.5**	**No**	**0.65**	**55.6**	**51.9**	**278.2**	**294.5**	**44.2**	**0.1**
Cyclopentane	2.93	8.5	10	196.8	**No**	0.6	73.5	53.9	287.3	315.8	70.6	0.14
Acetone	3.05	7	10	216.8	**n.a.**	0.64	88.4	79	413.7	435.5	58.9	0.1
Ethanol*	3.08	5	–	237.1	**Yes**	0.74	135.2	136.4	710.4	688	–	–
Methanol*	3.04	7.5	–	308.6	**Yes**	0.74	186.1	211.1	1063.2	960.3	–	–
Butanol	3.08	1.5	10	215.7	**Yes**	0.7	124.2	88.5	542.6	520	69.1	0.1
Hexane	2.75	7	10	191.1	**n.a.**	0.6	85.8	38.7	248.1	262.4	115	0.28
Heptane	2.78	3.5	10	190.9	**n.a.**	0.65	94.6	37.6	276.6	270.2	116.3	0.28
n-Pentane	2.46	14	10	189.5	**No**	0.41	76.2	38.6	171.5	101.8	110.4	0.26
Cyclohexane	3.05	4	10	189.4	**n.a.**	0.65	74.7	49.2	298	308.5	76.4	0.17

* No IHX recuperator is used for this fluid as it has a negative impact on COP, and 2 °C of superheating at evaporator outlet is assumed.

Even including the correlation of the compressor efficiency, fluorobenzene confirms its potentialities in HTHP delivering heat at 180 °C at high temperature lift, having the highest COP compared with the other candidates in Table T1.

References

[1] Naegler T, Simon S, Klein M, Gils HC. Quantification of the European industrial heat demand by branch and temperature level. Int J Energy Res 2015;39:2019–30. https://doi.org/10.1002/er.3436.

[2] Rehfeldt M, Fleiter T, Toro F. A bottom-up estimation of the heating and cooling demand in European industry. Energy Effic 2018;11:1057–82. https://doi.org/10.1007/s12053-017-9571-y.

[3] Alarnaot Alarnaout G, Navarro-Esbrí J, Mota-Babiloni A. Operational, economic, and carbon footprint feasibility of a moderately-high-temperature heat pump as an alternative to conventional boilers in various scenarios. Energy Convers Manag 2024;309:118424. https://doi.org/10.1016/j.enconman.2024.118424.

[4] Jouhara H, Żabnieńska-Góra A, Delpech B, Olabi V, El Samad T, Sayma A. High-temperature heat pumps: Fundamentals, modelling approaches and applications. Energy 2024;303:131882. https://doi.org/10.1016/j.energy.2024.131882.

[5] Arpagaus C, Bless F, Uhlmann M, Schiffmann J, Bertsch SS. High temperature heat pumps: Market overview, state of the art, research status, refrigerants, and application potentials. Energy 2018;152:985–1010. https://doi.org/10.1016/j.energy.2018.03.166.

[6] Mateu-Royo C, Navarro-Esbrí J, Mota-Babiloni A, Amat-Albuixech M, Molés F. Thermodynamic analysis of low GWP alternatives to HFC-245fa in high-temperature heat pumps: HCFO-1224yd(Z), HCFO-1233zd(E) and HFO-1336mzz (Z). Appl Therm Eng 2019;152:762–77. https://doi.org/10.1016/j.applthermaleng.2019.02.047.

[7] Mateu-Royo C, Navarro-Esbrí J, Mota-Babiloni A, Molés F, Amat-Albuixech M. Experimental exergy and energy analysis of a novel high-temperature heat pump with scroll compressor for waste heat recovery. Appl Energy 2019;253:113504. https://doi.org/10.1016/j.apenergy.2019.113504.

[8] Sulaiman AY, Cotter DF, Le KX, Huang MJ, Hewitt NJ. Thermodynamic analysis of subcritical High-Temperature heat pump using low GWP Refrigerants: A theoretical evaluation. Energy Convers Manag 2022;268:116034. https://doi.org/10.1016/j.enconman.2022.116034.

[9] Wolscht L, Knobloch K, Jacquemoud E, Jenny P. Dynamic simulation and experimental validation of a 35 MW heat pump based on a transcritical CO2 cycle. Energy 2024;294:130897. https://doi.org/10.1016/j.energy.2024.130897.

[10] Liu J, Zhang Y, Yin S, Zhang Y, Luo X, Liu Z. Economic and exergy transmission analysis of the gas-liquid type compressed CO2 energy storage system. Renew Energy 2024;230:120891. https://doi.org/10.1016/j.renene.2024.120891.

[11] Xu W, Zhao P, Ma N, Liu A, Wang J. Design and performance analysis of a combined cooling, heating and power system: Integration of an isobaric compressed CO2 energy storage and heat pump cycle. J Energy Storage 2024;91:112146. https://doi.org/10.1016/j.est.2024.112146.

[12] Liu Z, Zhang Y, Zhang Y, Su C. Performance of a high-temperature transcritical pumped thermal energy storage system based on CO2 binary mixtures. Energy 2024;305:132300. https://doi.org/10.1016/j.energy.2024.132300.

[13] Kontomaris K. HFO-1336mzz-Z: high temperature chemical stability and use as a working fluid in organic rankine cycles. Int Refrig Air Cond Conf 2014:10.

[14] Navarro-Esbrí J, Mota-Babiloni A. Experimental analysis of a high temperature heat pump prototype with low global warming potential refrigerant R-1336mzz(Z) for heating production above 155 °C. Int J Thermofluids 2023;17. https://doi.org/10.1016/j.ijft.2023.100304.

[15] Dai B, Liu X, Liu S, Wang D, Meng C, Wang Q, et al. Life cycle performance evaluation of cascade-heating high temperature heat pump system for waste heat utilization: Energy consumption, emissions and financial analyses. Energy 2022;261:125314. https://doi.org/10.1016/j.energy.2022.125314.

[16] Fox DB, Sutter D, Tester JW. The thermal spectrum of low-temperature energy use in the United States. Energy Environ Sci 2011;4:3731–40. https://doi.org/10.1039/C1EE01722E.

[17] Xin L, Liu C, Tan L, Xu X, Li Q, Huo E, et al. Thermal stability and pyrolysis products of HFO-1234yf as an environment-friendly working fluid for organic rankine cycle. Energy 2021;228:120564. https://doi.org/10.1016/j.energy.2021.120564.

[18] Liu J, Liu Y, Liu C, Xin L, Yu W. Experimental and theoretical study on thermal stability of mixture R1234ze(E)/R32 in organic rankine cycle. J Therm Sci 2023;32:1595–613. https://doi.org/10.1007/s11630-023-1790-2.

[19] Schlosser F, Zysk S, Walmsley TG, Kong L, Zühlsdorf B, Meschede H. Break-even of high-temperature heat pump integration for milk spray drying. Energy Convers Manag 2023;291:117304. https://doi.org/10.1016/j.enconman.2023.117304.

[20] Li S, Zhao Z, Zhang Y, Xu H, Zeng W. Experimental and numerical analysis of condensation heat transfer and pressure drop of refrigerant r22 in minichannels of a printed circuit heat exchanger. Energies 2020;13. https://doi.org/10.3390/en13246589.

[21] Obika E, Heberle F, Brüggemann D. Thermodynamic analysis of novel mixtures including siloxanes and cyclic hydrocarbons for high-temperature heat pumps. Energy 2024;294:130858. https://doi.org/10.1016/j.energy.2024.130858.

[22] Liu J, Zhou F, Lyu N, Fan H, Zhang X. Analysis of low GWP ternary zeotropic mixtures applied in high-temperature heat pump for waste heat recovery. Energy Convers Manag 2023;292:117381. https://doi.org/10.1016/j.enconman.2023.117381.

[23] Liu J, Zhou L, Lin Z, Zhang X. Performance evaluation of low GWP large glide temperature zeotropic mixtures applied in air source heat pump for DHW production. Energy Convers Manag 2022;274:116457. https://doi.org/10.1016/j.enconman.2022.116457.

[24] Klute S, Budt M, van Beek M, Doetsch C. Steam generating heat pumps – Overview, classification, economics, and basic modeling principles. Energy Convers Manag 2024;299:117882. https://doi.org/10.1016/j.enconman.2023.117882.

[25] IEA, IEA Annex 58, "enertime - High Temperature Heat Pump," (2023). https://heatpumpingtechnologies.org/annex58/wp-content/uploads/sites/70/2022/07/hthpannex58enertimetechnologyv2.pdf (accessed March 1, 2024).

[26] General Secretariat of the Council Delegations, Proposal for a Regulation of the European Parliament and of the Council on fluorinated greenhouse gases, amending Directive (EU) 2019/1937 and repealing Regulation (EU) No 517/2014, Brussels, 2002.

[27] Gaines LGT, Sinclair G, Williams AJ. A proposed approach to defining per- and polyfluoroalkyl substances (PFAS) based on molecular structure and formula. Integr Environ Assess Manag 2023;19:1333–47. https://doi.org/10.1002/ieam.4735.

[28] Abedini H, Vieren E, Demeester T, Beyne W, Lecompte S, Quoilin S, et al. A comprehensive analysis of binary mixtures as working fluid in high temperature heat pumps. Energy Convers Manag 2023;277:116652. https://doi.org/10.1016/j.enconman.2022.116652.

[29] Angelino G, Invernizzi C. General method for the thermodynamic evaluation of heat pump working fluids. Int J Refrig 1988;11:16–25. https://doi.org/10.1016/0140-7007(88)90007-2.

[30] Burkholder, O. Hondnebrog, B. McDonald, V.L. Orkin, V. Papadimitriou, D. Van Hoomissen, SUMMARY OF ABUNDANCES, LIFETIMES, ODPs, REs, GWPs, GTPs, (2023). https://tsapps.nist.gov/publication/get_pdf.cfm?pub_id=936562.

[31] Mills JE. The internal heat of vaporization. J Am Chem Soc 1909;31:1099–130. https://doi.org/10.1021/ja01940a001.

[32] Douslin DR, Moore RT, Dawson JP, Waddington G. The pressure-volume-temperature properties of fluorobenzene1. J Am Chem Soc 1958;80:2031–8. https://doi.org/10.1021/ja01542a001.

[33] Filippov LP. Liquid thermal conductivity research at Moscow University. Int J Heat Mass Transf 1968;11:331–45. -9310(68)90161-0. https://doi.org/10.1016/0017.

[34] S.P. Verevkin, V.N. Emel'yanenko, M.A. Varfolomeev, B.N. Solomonov, K. V. Zherikova, Vaporization enthalpies of a series of the fluoro- and chloro-substituted methylbenzenes, Fluid Phase Equilib. 380 (2014) 67–75. Doi: 10.1016/j.fluid.2014.07.029.

[35] Desreux V. A study of the parachor. Bull Des Sociétés Chim Belges 1935;44:249–87.

[36] Scott DW, McCullough JP, Good WD, Messerly JF, Pennington RE, Kincheloe TC, et al. Fluorobenzene: thermodynamic properties in the solid, liquid and vapor states; a revised vibrational assignment1. J Am Chem Soc 1956;78:5457–63. https://doi.org/10.1021/ja01602a001.

[37] Pasetti M, Invernizzi CM, Iora P. Thermal stability of working fluids for organic Rankine cycles: An improved survey method and experimental results for cyclopentane, isopentane and n-butane. Appl Therm Eng 2014;73:764–74. https://doi.org/10.1016/j.applthermaleng.2014.08.017.

[38] Angelino G, Invernizzi C. Experimental investigation on the thermal stability of some new zero ODP refrigerants. Int J Refrig 2003;26:51–8. https://doi.org/10.1016/S0140-7007(02)00023-3.

[39] Wang S, Li K, Yu W, Liu C, Guan Z. Effects of non-condensable gas on thermodynamic performance of transcritical organic Rankine cycle. Energy 2024;292:130513. https://doi.org/10.1016/j.energy.2024.130513.

[40] Li J, Gao G, Li P, Pei G, Huang H, Su Y, et al. Experimental study of organic Rankine cycle in the presence of non-condensable gases. Energy 2018;142:739–53. https://doi.org/10.1016/j.energy.2017.10.054.

[41] E. Macchi, M. Astolfi, Organic Rankine Cycle (ORC) Power Systems: Technologies and Applications, 2016.

[42] Benato A, Kærn MR, Pierobon L, Stoppato A, Haglind F. Analysis of hot spots in boilers of organic Rankine cycle units during transient operation. Appl Energy 2015;151:119–31. https://doi.org/10.1016/j.apenergy.2015.04.055.

[43] Invernizzi CM. Thermal stability evaluation for rankine cycles working fluids: experimental apparatus and calibration results. La Termotec N 1990;4:69–76.

[44] University of Brescia, ERGO - Fluid Test Laboratory, (n.d.).

[45] Invernizzi CM, Iora P, Manzolini G, Lasala S. Thermal stability of n-pentane, cyclopentane and toluene as working fluids in organic Rankine engines. Appl Therm Eng 2017;121:172–9. https://doi.org/10.1016/j.applthermaleng.2017.04.038.

[46] Invernizzi C, Binotti M, Bombarda P, Di Marcoberardino G, Iora P, Manzolini G. Water mixtures as working fluids in organic Rankine cycles. Energies 2019;12:1–17. https://doi.org/10.3390/en12132629.

[47] Lasala S, Invernizzi C, Iora P, Chiesa P, Macchi E. Thermal Stability Analysis of Perfluorohexane. Energy Procedia 2015;75:1575–82. https://doi.org/10.1016/j.egypro.2015.07.358.

[48] Di Marcoberardino G, Invernizzi CM, Iora P, Ayub A, Di Bona D, Chiesa P, et al. Experimental and analytical procedure for the characterization of innovative working fluids for power plants applications. Appl Therm Eng 2020;178:115513. https://doi.org/10.1016/j.applthermaleng.2020.115513.

[49] Sigma Aldrich, (n.d.). https://www.sigmaaldrich.com/IT/it (accessed February 28, 2024).

[50] Lecompte S, Oyewunmi OA, Markides CN, Lazova M, Kaya A, Van Den Broek M, et al. Case study of an organic Rankine cycle (ORC) for waste heat recovery from an electric arc furnace (EAF). Energies 2017;10:1–16. https://doi.org/10.3390/en10050649.
[51] Salogni A, Alberti D, Metelli M, Bertanzi R. Operation and maintenance of a biomass fired - Organic Rankine Cycle - CHP plant: the experience of cremona. Energy Procedia 2017;129:668–75. https://doi.org/10.1016/j.egypro.2017.09.141.
[52] Capra F, Martelli E. Numerical optimization of combined heat and power Organic Rankine Cycles - Part B: Simultaneous design & part-load optimization. Energy 2015;90:329–43. https://doi.org/10.1016/j.energy.2015.06.113.
[53] M. Gaia, 30 Years of Organic Rankine Cycle Development, First Int. Semin. ORC Power Syst. (2011) 29. http://orc2011.fyper.com/uploads/File/presentations3/30 Years of ORC development.pdf.
[54] enertime, ORC SOLUTIONS FOR INDUSTRY, (2023). https://www.enertime.com/assets/documents/fiche-orc_ind_7-2023_fr.pdf (accessed February 5, 2024).
[55] A. Foresti, Turboden: ORC Solutions for Cogeneration and District Heating, 2015.
[56] Turboden, Turboden ORC Technology Stands Out in Waste Heat Recovery Cement Plants, (2018). https://www.turboden.com/company/media/press/press-releases/2157/turboden-orc-technology-stands-out-in-waste-heat-recovery-cement-plants (accessed March 11, 2024).
[57] R.L. Cole, J.C. Demirgian, J.W. Allen, Predicting toluene degradation in organic Rankine-cycle engines, in: United States, 1987. https://www.osti.gov/biblio/6414474.
[58] V. Havens, D.R. Ragaller, Study of toluene stability for an Organic Rankine Cycle (ORC) space-based power system, in: 1988. https://api.semanticscholar.org/CorpusID:107906670.
[59] Study of Toluene Stability for an Organic Rankine Cycle Space-Based Power System, (1988).
[60] D.M. Ginosar, L.M. Petkovic, D.P. Guillen, Thermal Stability of Cyclopentane as an Organic Rankine Cycle Working Fluid, (2011) 4138–4144.
[61] Preißinger M, Brüggemann D. Thermal stability of hexamethyldisiloxane (MM) for high-temperature Organic Rankine Cycle (ORC). Energies 2016;9. https://doi.org/10.3390/en9030183.
[62] Keulen L, Gallarini S, Landolina C, Spinelli A, Iora P, Invernizzi C, et al. Thermal stability of hexamethyldisiloxane and octamethyltrisiloxane. Energy 2018;165:868–76. https://doi.org/10.1016/j.energy.2018.08.057.
[63] OSHA's Hazard Communication Standard, Safety Data Sheet - Fluorobenzene, 2019. https://www.agilent.com/cs/library/msds/STS-160-1_NAEnglish.pdf (accessed March 12, 2024).
[64] Júnior EPB, Arrieta MDP, Arrieta FRP, Silva CHF. Assessment of a Kalina cycle for waste heat recovery in the cement industry. Appl Therm Eng 2019;147:421–37. https://doi.org/10.1016/j.applthermaleng.2018.10.088.
[65] ECRA, Technical Report A-2016/1039: Evaluation of the energy performance of cement kilns in the context of co-processing, (2017) 53.
[66] Astolfi M, Macchi E. Efficiency correlations for axial flow turbines working with non-conventional fluids. Asme Orc 2015;2015:1–12.
[67] Peng DY, Robinson DB. A new two-constant equation of state. Ind Eng Chem Fundam 1976;15:59–64. https://doi.org/10.1021/i160057a011.
[68] Aspen Technology Inc., Aspen Plus®, Version V12.1, (2022).
[69] Jaatinen-Värri A, Honkatukia J, Uusitalo A, Turunen-Saaresti T. Centrifugal compressor design for high-temperature heat pumps. Appl Therm Eng 2024;239:122087. https://doi.org/10.1016/j.applthermaleng.2023.122087.
[70] Ganesan P, Eikevik TM. New zeotropic CO2-based refrigerant mixtures for cascade high-temperature heat pump to reach heat sink temperature up to 180 °C. Energy Convers Manag X 2023;20. https://doi.org/10.1016/j.ecmx.2023.100407.
[71] Dong Y, Wang R. When and how to use cascade high temperature heat pump—Its multi-criteria evaluation. Energy Convers Manag 2024;309:118435. https://doi.org/10.1016/j.enconman.2024.118435.
[72] J. Spale, A. Hoess, I.H. Bell, D. Ziviani, Low-GWP Working Fluid Mixtures Screening for Industrial High Temperature Heat Pumps with Supply Temperature $>$ 200 ° C Low-GWP Working Fluid Mixtures Screening for Industrial High Temperature Heat Pumps with Supply Temperature $>$ 200 ° C, in: 20th Int. Refrig. Air Cond. Conf. Purdue, 2024.